




Neuronal tau pathology worsens late-phase white matter degeneration after traumatic brain injury in transgenic mice

Fengshan Yu^{1,6} · Diego Iacono^{2,3,4,6} · Daniel P. Perl^{3,4,5} · Chen Lai^{5,6} · Jessica Gill⁷ · Tuan Q. Le¹ · Patricia Lee^{3,4,6} · Gauthaman Sukumar^{1,6} · Regina C. Armstrong^{1,5} 

Received: 26 May 2023 / Revised: 8 August 2023 / Accepted: 8 August 2023 / Published online: 14 August 2023
This is a U.S. Government work and not under copyright protection in the US; foreign copyright protection may apply 2023

Abstract

Traumatic brain injury (TBI) causes diffuse axonal injury which can produce chronic white matter pathology and subsequent post-traumatic neurodegeneration with poor patient outcomes. Tau modulates axon cytoskeletal functions and undergoes phosphorylation and mis-localization in neurodegenerative disorders. The effects of tau pathology on neurodegeneration after TBI are unclear. We used mice with neuronal expression of human mutant tau to examine effects of pathological tau on white matter pathology after TBI. Adult male and female hTau.P301S (Tg2541) transgenic and wild-type (Wt) mice received either moderate single TBI (s-TBI) or repetitive mild TBI (r-mTBI; once daily × 5), or sham procedures. Acutely, s-TBI produced more extensive axon damage in the corpus callosum (CC) as compared to r-mTBI. After s-TBI, significant CC thinning was present at 6 weeks and 4 months post-injury in Wt and transgenic mice, with homozygous tau expression producing additional pathology of late demyelination. In contrast, r-mTBI did not produce significant CC thinning except at the chronic time point of 4 months in homozygous mice, which exhibited significant CC atrophy (– 29.7%) with increased microgliosis. Serum neurofilament light quantification detected traumatic axonal injury at 1 day post-TBI in Wt and homozygous mice. At 4 months, high tau and neurofilament in homozygous mice implicated tau in chronic axon pathology. These findings did not have sex differences detected. Conclusions: Neuronal tau pathology differentially exacerbated CC pathology based on injury severity and chronicity. Ongoing CC atrophy from s-TBI became accompanied by late demyelination. Pathological tau significantly worsened CC atrophy during the chronic phase after r-mTBI.

Keywords Neuroregeneration · Traumatic brain injury · White matter · Tau · Demyelination · Axon damage

✉ Regina C. Armstrong
regina.armstrong@usuhs.edu

- 1 Department of Anatomy, Physiology and Genetics, School of Medicine, Uniformed Services University of the Health Sciences, 4301 Jones Bridge Rd, Bethesda, MD 20814, USA
- 2 Neurology, Uniformed Services University of the Health Sciences, Bethesda, MD, USA
- 3 Pathology, Uniformed Services University of the Health Sciences, Bethesda, MD, USA
- 4 Department of Defense-Uniformed Services University Brain Tissue Repository, Uniformed Services University of the Health Sciences, Bethesda, MD, USA
- 5 Center for Neuroscience and Regenerative Medicine, Uniformed Services University of the Health Sciences, Bethesda, MD, USA
- 6 Henry M. Jackson Foundation for the Advancement of Military Medicine, Uniformed Services University of the Health Sciences, Bethesda, MD, USA
- 7 Johns Hopkins University, Baltimore, MD, USA

Introduction

Traumatic brain injury (TBI) can lead to post-traumatic neurodegeneration of gray and white matter brain regions that is associated with poor patient outcomes [9, 34]. More specifically, diffuse axonal injury in the corpus callosum is associated with post-traumatic neurodegeneration and unfavorable functional outcomes, as measured using the Glasgow Outcome Scale (GOS) or the Glasgow Outcome Scale-Extended (GOSE) [34, 83]. Post-traumatic neurodegeneration can result from progressive secondary pathology following a single moderate-severe TBI or from milder repetitive concussive and subconcussive injuries. Secondary processes that contribute to post-traumatic neurodegeneration are important to identify and warrant high priority as therapeutic targets to mitigate the detrimental effects of TBI on long-term brain health [12].

The purpose of this study was to test neuronal tau pathology as a contributing factor in the post-traumatic degeneration of white matter tracts that exhibit traumatic axonal injury, a hallmark pathology of TBI. Degeneration of cerebral white matter, including the atrophy of the corpus callosum, has long been recognized in postmortem cases after a single moderate-severe TBI [44, 76]. Recent magnetic resonance imaging (MRI) studies reveal that focal damage to densely connected white matter regions of brain networks results in worse cognitive impairment than similar damage to gray matter hubs [51, 64]. Furthermore, MRI parameters of white matter diffuse axonal injury predict subsequent white matter atrophy as well as whole brain atrophy over time after moderate-severe TBI [33]. Post-traumatic white matter atrophy involves deep white matter, e.g., corpus callosum and corticospinal tracts, which are associated with axonal damage [32]. A plasma biomarker of axonal damage, neurofilament light protein, correlates with MRI measures of diffuse axonal injury and predicts both chronic phase white matter neurodegeneration and functional outcomes after TBI [34, 61]. Brain atrophy, including reduced corpus callosum volume, and higher plasma neurofilament light levels have also been found after repetitive TBI in boxers [7]. Similarly, repetitive sports related head injuries diagnosed by neuropathology as chronic traumatic encephalopathy (CTE) exhibit post-traumatic neurodegeneration with cerebral atrophy that includes white matter changes of corpus callosum thinning, myelin rarefaction, axon loss, and altered glial phenotypes [3, 15, 19].

Neuronal phosphorylated tau pathology has been implicated in secondary injuries after TBI due to association with neurodegenerative diseases and being observed in postmortem cases of CTE as well as after single events of more severe TBI [19, 38, 71, 84, 86]. In the healthy adult brain, tau is localized in axons and serves as a microtubule-associated protein that modulates axonal transport and stability of the axon cytoskeleton [72, 82, 92]. Tau localization in axons and binding to microtubules is regulated by phosphorylation [72, 92]. A range of genetic and acquired conditions can lead to tau hyperphosphorylation, mis-localization, aggregation and/or impaired clearance [11, 38, 40, 41]. Such findings indicate potential interplay between TBI sequelae and tau pathology in the progression of white matter degeneration that remains poorly understood.

In this study, we tested the effect of increasing levels of neuronal tau pathology on the progression of white matter degeneration after a moderate single TBI (s-TBI) or after repetitive mild TBI (r-mTBI) in transgenic mice expressing human tau with a pathogenic mutation. Varied pathology, particularly the extent of corpus callosum axon damage in these two different injury models, was tested relative tau transgene dosage to inform interpretation of heterogeneous patient populations. As extensively characterized in adult

wild-type mice, the s-TBI model produces traumatic axonal injury that progresses to corpus callosum atrophy, with features that model clinical findings of neuropathology and MRI of patients with TBI [10, 33, 54, 56, 63, 73]. Similarly, the r-mTBI model has also been previously characterized in wild-type mice using neuropathology and MRI [90]. The r-mTBI model uses a milder impact separated by 24 h across 5 consecutive days, which produces traumatic axonal injury at acute and subacute time points, but does not degenerate so far as to produce overt corpus callosum atrophy [62, 90]. Progressive tau pathology pertinent to human histopathology has been demonstrated in adult wild-type mice in recent studies that also used a 5-day repetitive mild head injury, along with interpretations from a systematic review of prior literature [45].

Prior studies in wild-type and human tau transgenic mice have advanced our knowledge of the molecular mechanisms of tau pathology and informed our use of human tau transgenic mice for analysis of post-traumatic neurodegeneration [5, 31, 45, 84]. Supplemental Table SI-1 lists examples of specific studies that are particularly relevant to the purpose of the current study. Although the hTau mouse line enabled expression of all six isoforms of human tau driven from the human tau promoter [4], only hemizygous hTau mice are viable and the level of human tau expressed did not alter the neuropathological sequelae of TBI [27, 58]. We use hTau.P301S (Tg2541) mice that, although leveraging a human mutation to generate tau pathology, offer multiple advantages for the current studies of phosphorylated tau pathology as contributing to post-traumatic neurodegeneration. Tg2541 mice express the P301S mutation of the human tau gene driven in neurons from the Thy1.2 promoter [2]. Using Thy1-YFP-16 mice, we previously demonstrated that neurons expressing a fluorescent reporter protein from the Thy1.2 promoter exhibit axon damage in the corpus callosum and cerebral cortex in both s-TBI and r-mTBI models, with the most prominent axon damage in the corpus callosum after the moderate s-TBI [54, 90]. The Tg2541 mice have more reproducible tau expression than hTau.P301S (PS19) mice, which have extensive variability in both the rate of tau spreading and phosphorylated tau pathology [85]. Interestingly, studies in Tg2541 mice revealed molecular interactions that regulate phosphorylated tau pathology in the adult forebrain [43], which may indicate the potential for modulation by TBI sequelae. Furthermore, recent phosphoproteomics analysis in Tg2541 mice identified protein co-expression modules that correspond with cellular responses to phosphorylated tau pathology [81]. These findings in Thy1-YFP-16 mice and Tg2541 mice support our current study design and inform future studies of the cellular and molecular basis of tau effects in TBI models.

In the current study, we first confirmed in the Tg2541 line that the moderate s-TBI produces more extensive axon

damage based on neuropathology. We also validated expression of reproducible differences in human tau protein in brain lysates from regions under the impact site, i.e., the rostral corpus callosum and cerebral cortex, with significant gene dosage effects across wild-type, hemizygous (Hemi), and homozygous (Hom) mice generated from the Tg2541 colony. We then conducted clinically relevant neuropathologic and blood biomarker assessments of the Tg2541 genotype effect at acute (1 day), subacute (6 weeks) and chronic (4 months) phases after s-TBI and r-mTBI. This translational approach demonstrated that phosphorylated tau pathology, axon damage, neuroinflammation, demyelination, and corpus callosum atrophy progressed with distinctly different timing and extent based upon the injury parameters in combination with the human mutant tau gene dosage.

Methods

hTau.P301S (Tg2541) mice

All animals were treated in accordance with guidelines of the National Institutes of Health Guide for the Care and Use of Laboratory Animals. The study protocol was approved by the Institutional Animal Care and Use Committee of the Uniformed Services University of the Health Sciences. Mutant human tau transgenic mice (B6-Tg(Thy1-MAPT*P301S)2541), also known as hTau.P301S (Tg2541) or Tg2541 mice, were generated by Dr. Goedert [2] with breeders backcrossed with C57BL/6J mice, and generously provided by Dr. Tony Wyss-Coray (Stanford University, Palo Alto, CA). This hTau.P301S Tg2541 line expresses a transgene of the Thy1.2 promoter driving neuronal transcription of the P301ShTau43 construct which encodes the shortest human four repeat-tau isoform (383 aa isoform of human Tau; 0N4R) with a P301S mutation (Supplemental Information Table SI-1). Hemizygous mice were bred at the Uniformed Services University of the Health Sciences to generate experimental mice. Mice were housed in standard cages in a 12-h/12-h light–dark cycle with food and water ad libitum. Breeding and experimental procedures were conducted from January 2016 through September 2021.

DNA from mouse ear biopsies was used for genotyping with quantitative PCR using primer pairs for both the inserted vector sequence (5'-AAAGGAAGTCAACTCCACCTCAC-3' and 5'-ACCTTACTGAGCTAGCAGGTCTTT-3') and for the mutant human MAPT 5'-(GATTGGGTCCTGGACAATA-3' and 5'-GTGGTCTGTCTTGGCTTTGG-3'). In addition, early in establishing the colony, some mice were genotyped for HuMAPT mut detection using DNA from tail biopsies with analysis by Transnetyx (Memphis, TN) using primers pair of 5'-CAGGAGTTCGAAGTG

ATGGAAGA-3' and 5'-AGCCCCCCTGATCTTTCCT-3' with reporter CCCGTACGTCCCAGCGTG.

Traumatic brain injury procedures

Two different models of TBI were used to reflect different human injuries associated with tau pathology and post-traumatic neurodegeneration. Both male and female mice were used for sham or TBI procedures at 8 weeks of age. An Impact One Stereotaxic Impactor (Leica Biosystems, Deer Park, IL) was used to produce concussive models of repetitive mild TBI (r-mTBI) [90] or single moderate TBI (s-TBI) [54, 56, 77], as previously characterized to produce pathology in the rostral corpus callosum and medial cerebral cortex. Mice were anesthetized with 2.0% isoflurane in O₂ and positioned in a stereotaxic frame with the head fixed with ear bars capped by rubber stoppers for s-TBI and r-mTBI procedures. The impacts were made at stereotaxic coordinates for bregma (0 ML, 0 AP, 0 DV) using a 3-mm diameter tip with a flat surface and rounded beveling of the edge (Cat# 2530-3S, Neuroscience Tools, Aurora, IL). For s-TBI, after depilation of the scalp hair with Nair, a midline incision was made to expose skull and impact was made onto the intact skull at bregma (velocity at 4.0 m/s; depth of 1.5 mm; dwell time of 100 ms). For r-mTBI, after shaving and depilation of the scalp hair, impacts (velocity at 4.0 m/s; depth of 1.0 mm; dwell time of 200 ms) were made onto the scalp approximately over bregma. The r-mTBI consisted of 5 impacts with one per day at 24-h intervals on 5 consecutive days. Sham mice underwent identical procedures to their respective TBI mice without receiving impacts. To mitigate potential pain experienced from the injury procedures, mice were given acetaminophen (1 mg/ml) in the drinking water starting the day before a TBI or sham procedure and returned to standard drinking water one day after the final procedure. Body temperature was maintained with a warming pad. After each procedure, the duration of apnea and the righting reflex were recorded. The righting reflex was measured immediately after removal from anesthesia and placement of the mouse in the supine position to righting to the prone position, which is a surrogate measure of transient alteration of consciousness after TBI.

Immunohistochemistry and histological staining

Mice were perfused with 0.1 M phosphate buffer followed by 4% paraformaldehyde at 1 day, 6 weeks, or 4 months after TBI and sham procedures. Brains and spinal cords were dissected and further post-fixed by immersion in the same fixative overnight. Tissues were embedded in paraffin and then cut as coronal Sects. (5 μm). Immunohistochemistry was used to detect tau and cell type specific markers with antibodies listed in Table 1. Briefly, HT7 detected human

Table 1 Antibody information

Application	Primary antibodies	Secondary antibodies
IHC	HT7 (mouse monoclonal) 1:150 Thermal Fisher Cat # MN1000 RRID: (AB_231465) AT8 (mouse monoclonal) 1:200 Thermal Fisher Cat # MN1020 RRID: (AB_223647) Iba1 (rabbit monoclonal) 1:200 FUJIFILM Wako Pure Chemical Corporation Cat # 019-19741 RRID: (AB_839504) GFAP (rabbit polyclonal) 1:100 DAKO Cat # GA524 RRID: (AB_2811722) β -APP (mouse monoclonal) 1:100 Millipore Sigma Cat # MAB348 RRID: (AB_94882) SMI-34 (mouse monoclonal) 1:100 Biologend Cat # 835503 RRID: (AB_2572004) MBP (rat monoclonal) 1:100 Abcam Cat # AB7349 RRID: (AB_305869)	Secondary antibodies inside the diaminobenzidine chromogen detection system (Leica Biosystems, DS9800)
Wes	HT7 (mouse monoclonal) 1:1000 Thermal Fisher Cat # MN1000 RRID: (AB_231465) AT180 (mouse monoclonal) 1:50 Thermal Fisher Cat # MN1040 RRID: (AB_223649) P-Tau (S404) (rabbit polyclonal) 1:1000 Thermal Fisher Cat # 44-758G RRID: (AB_2533746) P-Tau (T205) (rabbit polyclonal) 1:200 Thermal Fisher Cat # 44-738G RRID: (AB_2533738)	Goat Anti-Mouse Secondary HRP Protein Simple Cat # 042-205 RRID: (AB_2860576) Goat Anti-Mouse Secondary HRP Protein Simple Cat # 042-205 RRID: (AB_2860576) Goat Anti-Rabbit Secondary HRP Protein Simple Cat # 042-206 RRID: (AB_2860577) Goat Anti-Rabbit Secondary HRP Protein Simple Cat # 042-206 RRID: (AB_2860577)

Tau isoforms while AT8 immunolabeled tau phosphorylated at S202/T205. Microglia were identified based on ionized calcium-binding adaptor molecule 1 (IBA1) immunoreactivity. Astrocytes were immunolabeled for glial fibrillary acidic protein (GFAP). Axon damage was evaluated based on beta-amyloid precursor protein (β -APP) or phosphorylated neurofilament H (SMI-34) antibodies. Myelination was immunolabeled for myelin basic protein (MBP). Immunohistochemistry was performed analogous to the human TBI neuropathology processes, using Leica Bond III automated staining system with diaminobenzidine chromogen detection and the same antibodies as for clinical diagnostics (DS9800, Leica Biosystems, Buffalo Grove, IL). Hematoxylin and eosin stain was used for general histopathology. Sections were scanned to create digital images with either NanoZoomer (Hamamatsu Photonics, Japan) or Aperio (Aperio AT2—High Volume, Digital whole slide scanning scanner, Leica Biosystems, Deer Park, IL) digital slide scanning systems and images were captured and exported with NDP viewer (Hamamatsu Corporation) or Aperio ImageScope (Leica Biosystems), respectively.

Quantification of immunohistochemistry and histological staining was conducted with coronal sections from within approximately +0.5 to –0.5 mm of bregma (i.e., under impact site). The corpus callosum region-of-interest included both hemispheres extending laterally over the lateral ventricle and under the peak of the cingulum. The

medial cerebral cortex was analyzed for the cingulate and motor cortex above the corpus callosum region [90]. Reactive astrogliosis and microgliosis were estimated from the area of immunoreactivity for GFAP or IBA1 using ImageJ (NIH, Bethesda, MD). Damaged axons in the corpus callosum or medial cerebral cortex were counted manually using NIH ImageJ (NIH) with β -APP or SMI-34 images, respectively, based on the presence of large terminal end bulbs or as multiple swellings along a longitudinal axonal profile. Any β -APP or SMI-34 positive end bulb that was adjacent to or continuous with a nucleus was excluded. For quantification of axon damage, the hematoxylin nuclear counterstain was used to exclude immunolabeling associated with neuronal or glial cell bodies [28, 35]. Corpus callosum width was analyzed with hematoxylin and eosin staining or with immunolabeling for MBP. The width was calculated for each mouse from the average of 7 measurements (midline, and bilaterally approximately 200 μ m from midline, under the peak of cingulum, and at the lateral border of ventricle [54, 56], using images digitized at 20 \times on NDP viewer (Hamamatsu Corporation) or Aperio ImageScope (Leica Biosystems). Myelination was estimated from the area of MBP immunoreactivity analyzed with Image J in the corpus callosum region-of-interest, as defined above, and within the motor cortex area of myelinated fibers (box drawn as 200 μ m medial, 200 μ m lateral, and 200 μ m superior as measured from cingulum peak). HT7 immunolabeling was used to

identify the presence or absence of human tau expression. Analysis of AT8 scored immunoreactivity, based on intensity and area, as negative or present (scale of + to +++) to localize phosphorylated mouse or human tau in tissue sections as a complement to Wes quantification of tau protein in brain lysates (see below).

Soluble tau protein and phospho-tau epitopes in brain lysates

Soluble tau in brain tissue was quantified with Wes Protein Simple Westerns™ (Protein Simple, San Jose, CA). Prior to tissue collection, mice were perfused with cold phosphate buffered saline (PBS) to flush out blood. The brain was cut rapidly with McIlwain Tissue Chopper (Stoelting Co., Wood Dale, IL) into 1 mm thick coronal slices and placed in cold PBS. The slice containing the anterior commissure was identified to estimate the slice aligned in the coronal plane with bregma. The upper forebrain was quickly dissected by a straight razor cut in the horizontal plane just below the lowest midline point of corpus callosum. This upper forebrain region under the impact site included the corpus callosum and cerebral cortex at coronal levels from two slices comprising approximately + 1.0 mm to – 1.0 mm relative to bregma. Tissue was stored in – 80 °C freezer. The soluble protein fraction was isolated with minor modifications of published protocols [20] [87]. Brain tissue samples were immersed in 3 X T-per buffers (#78510; Thermo Fisher, Waltham, MA) with protease and phosphatase inhibitors (#1861281; Thermo Fisher). After homogenization and sonication, the tissue suspension was separated at 80000g, 4 °C for 30 min in an Optima™ MAX Ultracentrifuge (Beckman, Germany). Supernatant was collected and stored at – 80 °C. Simple Westerns™ (Wes Protein Simple) were run according to the manufacturer's protocol. Primary antibodies used and their conditions are listed in Table 1. Data were analyzed with Compass software (Protein Simple). A peak on the electropherogram is accepted when the molecular weight is at the right position, and signal to noise ratio is higher than 10. All the peaks wider than 20 were excluded.

Serum biomarkers

Mouse serum was analyzed for biomarkers using the ultra-sensitive Single molecule array (Simoa ®) for the Neurology 4-Plex A multiplex assay (N4PA; Quanterix, Lexington, MA), as has been successfully used in clinical studies [29, 47, 49]. Cardiac blood was collected as a terminal procedure from the mice utilized in other experiments of this study. Blood was drawn from the right atrium of deeply anesthetized mice immediately before intraventricular perfusion. After remaining undisturbed at room temperature for at least 30 min, samples were centrifuged at 3000g for 10 min.

Serum were carefully collected and stored at – 80 °C until analyzed. Serum levels of tau, GFAP, neurofilament light chain (Nf-L) and Ubiquitin C-terminal Hydrolase-1 (UCHL-1) levels were simultaneously measured in each sample and samples were run in duplicate on a Simoa ® HD-1 Analyzer (Quanterix, Lexington, MA). The results with coefficient of variation values below 10% were accepted for final analysis. This assay is designed for detection of human proteins. Performance with mouse proteins in serum was tested by the manufacturer (Quanterix application note MKT-0038 01). Immunodepletion tests demonstrated good specificity for mouse Nf-L and that the assay does not have specificity for detecting mouse GFAP or UCHL-1 proteins, in agreement with our results (data not shown).

Progression of neurologic impairment

In this line of hTau.P301S Tg2541 mice, phosphorylated tau pathology initiates in the spinal cord and mice develop corresponding paresis and paralysis with age [2]. Therefore, the hang time test was used to quantify early spinal cord dysfunction [26, 65]. Briefly, the mouse was placed onto a wire cage top held over the padded surface. The cage top was then inverted so that the mouse gripped the wire bars to support its own weight. The time hanging onto the cage top was recorded for up to 60 s. Mice with spinal cord pathology, including limb paralysis or paresis, do not have the grip strength to support their weight for 60 s and so drop to the padding at different time intervals depending upon the severity of the neuromuscular effect. Healthy adult C57BL/6 mice can hold on for the maximum trial time of 60 s without any difficulty, while mice that do not hang onto the cage bars for at least 30 s are considered impaired [26]. Hang time scores were calculated as the average of three hang time trials conducted in series with 15 s intervals to rest. After the hang time testing, mice were also observed for signs of limb paresis and paralysis with a neurological deficit score of 1 assigned for each affected limb up to a total score of 5 (limbs and/or tail).

Mouse numbers and data analysis

The experiments involved a total of 636 mice, including males and females, which required different tissue collection so that 468 mice were perfused for immunohistochemistry and 168 mice were prepared for protein quantification of brain lysates. Among these mice, 69 non-injured (naïve) mice were evaluated with the hang time test to select post-injury time points relative to the progression of neurological deficits with the tau phenotype, 150 had behavioral testing based on sociability impairment, and cardiac blood was collected from 491 mice as part of the terminal procedure for the tissue analysis. Experiments included approximately

equal numbers of male and female mice based on the combination across cohorts of experimental mice available in litters from hemizygous breeders. The number of mice of each sex for each condition in each experiment is shown in a table (see Supplemental Information) that is cited in each figure legend. Mice were allocated to sham or injured to distribute available mice to both conditions and balance sexes, to the extent possible within each litter. Most litters did not have sufficient mice for further steps to randomize within a sex and condition. Mice were allocated to injury or sham conditions prior to 8 weeks of age, which precedes behavioral signs associated with the tau phenotype. Mouse weights did not vary due to genotype at 8 weeks of age (data not shown). Experiments for the single impact TBI and corresponding sham condition have a visible scalp incision while the repetitive TBI and corresponding sham condition do not have a scalp incision; therefore, experiments in each model were conducted separately and were not randomized within cohorts. Mice were excluded if the injury procedure inadvertently produced a depressive skull fracture, or if the mice had poor health to require euthanasia or otherwise died prior to the experimental endpoint. Humane euthanasia was required for mice that developed severe paraparesis. Power analysis for quantification of neuropathology in tissue sections was estimated from prior studies. However, the tissue analysis as defined by specific region-of-interest was important to maintain, so mice had to be excluded if sufficient tissue was no longer available. The Cohen's *d* effect size is provided for the major findings of the neuropathology using the myelin basic protein immunohistochemistry results that had a low sample number. Quantitative analysis was based on values for each individual mouse for each condition so that values for each mouse are shown by symbols on the graphs for each experiment. All assessments were performed with blinding as to the mouse injury and tau genotype.

All data analysis was performed with GraphPad Prism 8 software (GraphPad Software, Inc., La Jolla, CA). Two-way analysis of variance (ANOVA) with post hoc Holm–Sidak's multiple comparisons test was used for statistical comparison of tau genotype and injury effects for the data from neuropathology of tissue sections, Wes Protein Simple and serum biomarkers. Neurological impairment based on the hang time test was analyzed as a Kaplan–Meier plot with the Mantel–Cox log rank test for statistical comparison. The full set of statistical comparison data is provided as tables in the Supplemental Information that are referred to in each figure legend. Statistically significant post hoc comparisons are also shown on the graphs for each experiment. Statistical significance was defined as $p < 0.05$.

Results

Acute injury severity is greater in s-TBI than r-mTBI at 8 weeks of age and is not increased by tau genotype

The study design took advantage of the distinct progression of neurologic impairment with hTau.P301S gene dosage in the Tg2541 mice (Fig. 1). Homozygous mice are expected to develop overt neurologic symptoms of muscle weakness, tremor, and severe paraparesis at 5–6 months of age with a similar phenotype in hemizygous mice by 12–14 months [2]. We quantified the onset of neurologic symptoms with aging in non-injured (naïve) mice using a hang time test of grasping and strength each month (Fig. 1a). In homozygous mice, hang time deficits developed by 4–6 months of age and progressed to paraparesis by 7–8 months of age. Based on this neurologic progression, the study was designed for mice to receive head injuries at 8 weeks of age with survival for 1 day (acute), 6 weeks (subacute), and 4 months (chronic) after injury or sham procedures (Fig. 1a, b). This time course targeted analysis at the acute and subacute phases prior to the onset of symptoms and at the chronic phase after symptom onset indicative of progressive pathology in homozygous mice for comparison with hemizygous and wild-type littermates.

This time point of 8 weeks of age at the time of injury is matched to our prior studies characterizing the distinct s-TBI and r-mTBI injury models using neuropathology, electron microscopy, MRI, and behavior analyses [10, 54, 56, 63, 90]. The acute phase post-surgical and neuropathology data from these prior studies are similar to the results in the Tg2541 mice across wild-type, hemizygous, and homozygous genotypes. Parameters of acute injury severity were increased in the moderate s-TBI model as compared to the r-mTBI model (Fig. 1c–e). Immediately after the injury or sham procedures, the s-TBI produced a longer delay than the r-mTBI in righting reflex, which is a surrogate measure for loss of consciousness (Fig. 1c). The delay in righting time was significantly increased in injured mice relative to the sham condition in both the s-TBI and r-mTBI models, and was not altered across tau genotypes (Fig. 1c and SI-2; Table SI-5). The delay for s-TBI is compared with the first of the five days of r-mTBI impacts since this first day consistently produced the longest righting reflex time interval (Fig. SI-2; Table SI-5).

Acute axon damage was quantified at 24 h after the s-TBI impact or the last of five r-mTBI impacts using immunolabeling for β -amyloid precursor protein (APP), as in our prior studies in each model [77, 90]. APP immunolabeling detects early stage axon damage associated with

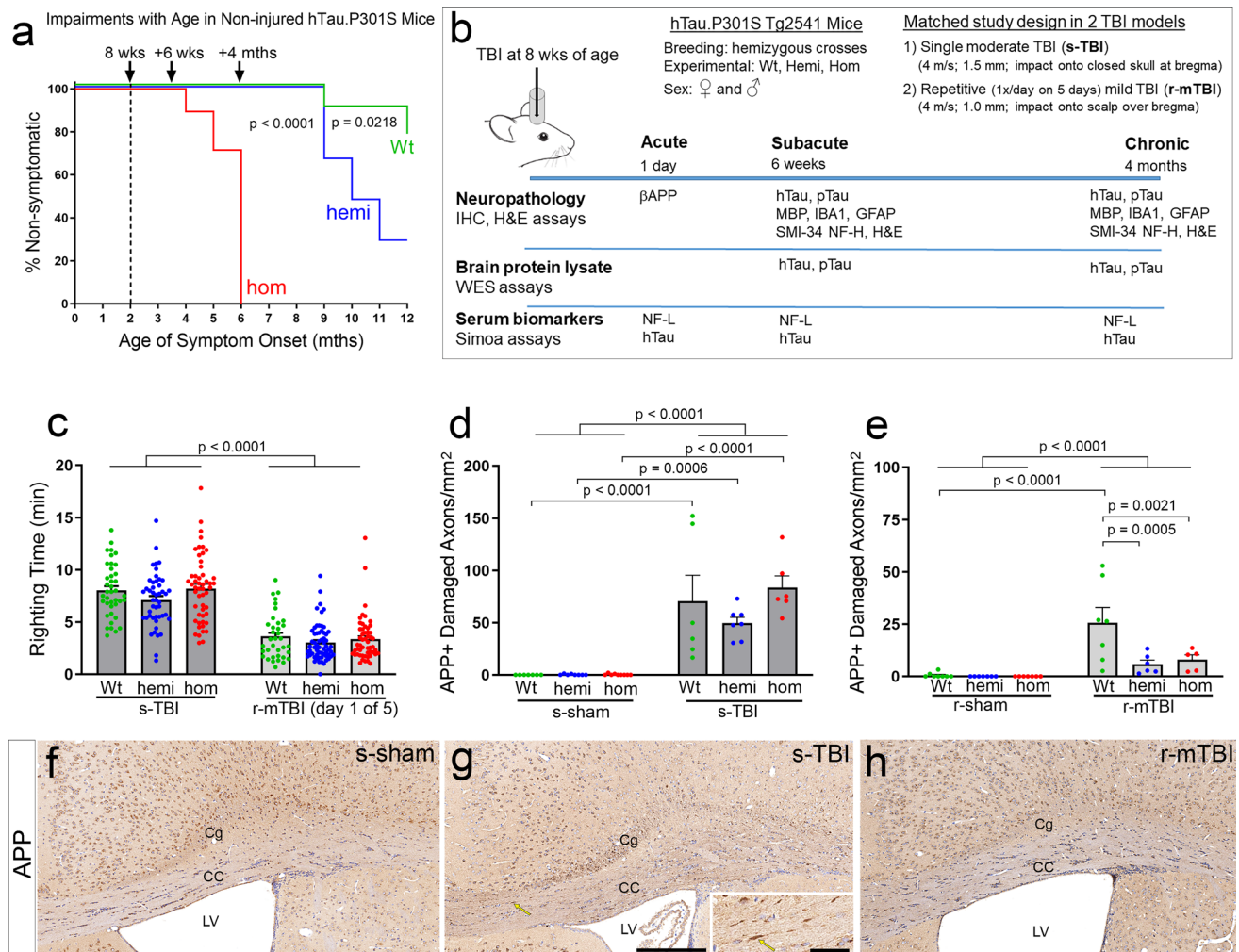


Fig. 1 Acute injury severity is greater in s-TBI than r-mTBI and is not increased by hTau.P301S genotype at 8 weeks of age, prior to tau-induced neurologic impairment. **a** The ability of non-injured (naïve) mice to support their weight while hanging from wire cage top bars reveals progressive neurologic impairment with increasing age that is accelerated in homozygotes. This time course in naïve mice was used to select the time points for analysis after TBI. **b** The study design matches mice across genotype, sex, and TBI models for differential comparisons at phases prior to and after symptom onset. Three distinct approaches examine tau expression for localization, quantification, and translational biomarkers. **c** Immediately after TBI or sham procedures, a surrogate measure of loss of consciousness is an indicator of more severe injury after s-TBI compared to r-mTBI across genotypes. See also Fig. SI-2 for comparison of sham and injured for each genotype. **d** At 24 h after a single moderate TBI (s-TBI), acute axon damage in the corpus callosum is increased across genotypes. **e** At 24 h after the last impact in the repetitive mild TBI (r-mTBI), the acute axon damage is highest in wild-type mice

yet less extensive than in s-TBI mice (Fig. SI-3). **c–e** Dots represent individual mice with wild type (Wt) in green, hemizygous (hemi) in blue, and homozygous (hom) in red. Non-significant comparisons are not shown. See Supplemental Information for full statistical analysis of this data along with analysis showing that sex differences were not observed in the righting reflex (Table SI-5), APP immunolabeling (Tables SI-6, SI-7), or hang time results (Table SI-2) even though sex differences were observed among the weights collected for non-injured mice used in the hang time testing (Fig. SI-1; Table SI-3). **f–h** Representative images of β-APP immunolabeling in the corpus callosum (CC) area under the impact site in wild-type mice from the Tg2541 line. Damaged CC axons were identified as β-APP immunolabeled swellings in longitudinal axon profiles (G, yellow arrow enlarged in inset). After s-TBI, damaged axons are also evident in the cingulum (Cg) as β-APP accumulated in transverse axon profiles. Hematoxylin staining of nuclei (blue) was used to exclude β-APP associated with neuron and glial cell bodies. LV lateral ventricle. Scale bars: f–h shown in g = 200 μm, inset = 50 μm

impaired axonal transport, axonal fragmentation, and formation of terminal end bulbs (Fig. 1d–h). As compared to the sham condition, significant CC axon damage resulted from s-TBI (Fig. 1d, f, g) and r-mTBI (Fig. 1e, h). Acute axonal injury was significantly more extensive after s-TBI

as compared to the r-mTBI in mice of all three genotypes (Figs. 1d, e and SI-2). Furthermore, the tau genotype did not increase acute vulnerability to axon damage with s-TBI or r-mTBI at 8 weeks of age (Fig. 1d, e). The lack of a detrimental effect of tau genotype after acute injury is an

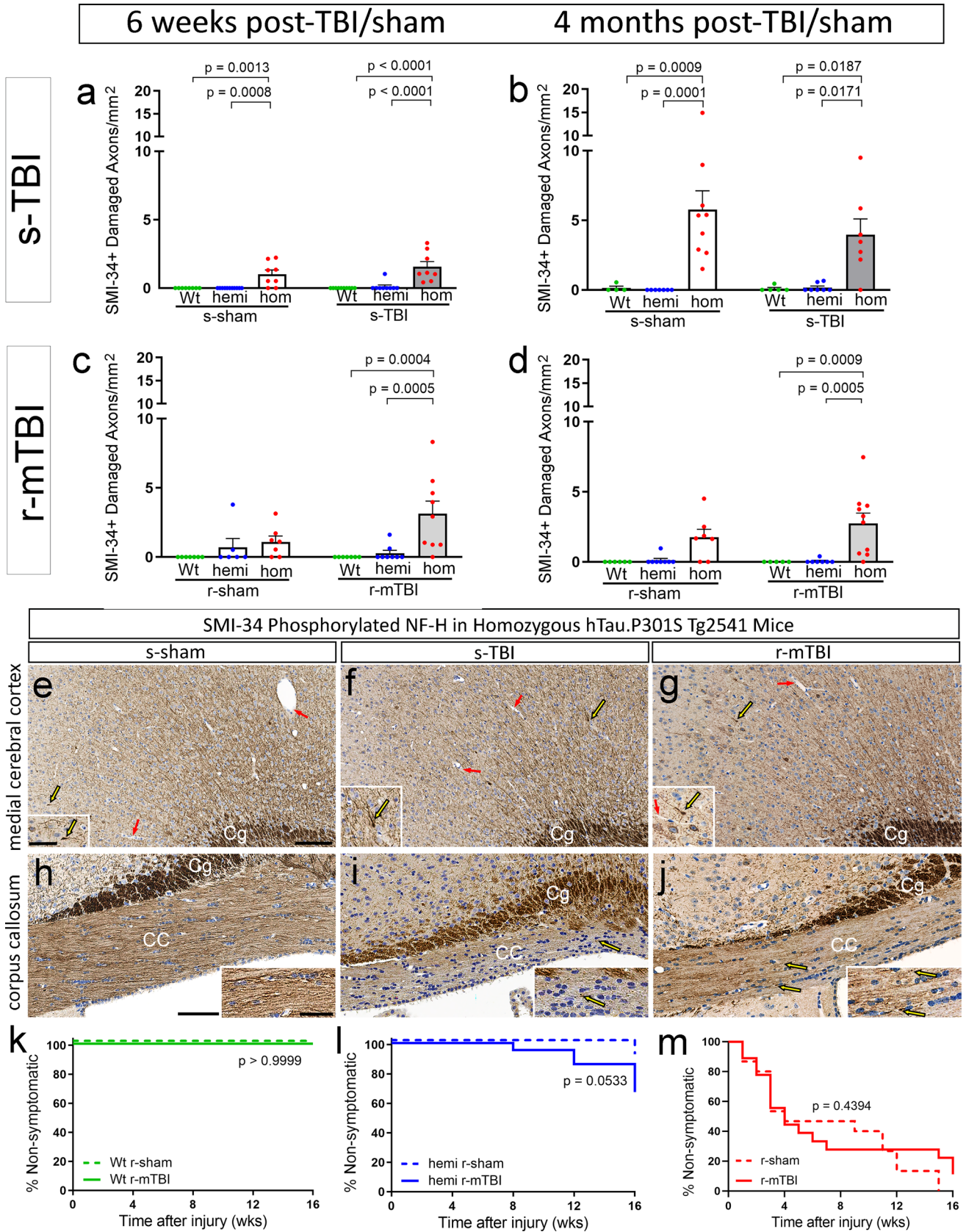


Fig. 2 Homozygous hTau.P301S genotype increases cortical axon damage at subacute and chronic stages. **a–d** Damaged axons with swellings or endbulbs identified with SMI-34 phosphorylated neurofilament immunolabeling in the medial cerebral cortex under the impact site at 6 weeks (subacute) or 4 months (chronic) stages after TBI or sham procedures. Dots represent individual mice with wild type (Wt) in green, hemizygous (hemi) in blue, and homozygous (hom) in red. Non-significant comparisons are not shown. **a–e** Axon damage is significantly increased in only homozygous mice after s-TBI or the s-sham procedure, which involves anesthesia and scalp incision. **c, d** Axon damage is increased only in homozygous mice after r-mTBI, but is not increased after the r-sham procedure that involves only anesthesia. **e–j** Representative images of SMI-34 immunolabeling in regions under the impact site in coronal brain sections from homozygous mice at 4 months after TBI or sham procedures. Yellow arrows indicate examples of damaged axons in the medial cortex and corpus callosum (CC) that are enlarged in each inset. Axons cut transversely in the cingulum (Cg) are strongly immunolabeled. Red arrows indicate examples of blood vessels, which are not SMI-34 immunolabeled. Nuclei stained blue with hematoxylin. Scale bars: **e–g** shown in $e = 100 \mu\text{m}$, **h–j** shown in $h = 100 \mu\text{m}$, insets shown in $h = 50 \mu\text{m}$. **k–m** Neurologic deficits on the hang time test are not significantly different after r-mTBI as compared to sham procedures in mice of each genotype. See Supplemental Information for full statistical analysis of this data along with analysis showing a sex difference only for the hemizygous mice after r-mTBI (Table SI-4), and no sex differences in the SMI-34 groups (Tables SI-6, SI-7)

important finding for attributing tau effects at subacute and chronic time points in the subsequent experiments of this study design.

Cortical axon damage is increased at subacute and chronic stages in tau homozygous mice

After the acute injury stage, a specific increase in axon damage due to tau genotype was evident as homozygous mice aged to subacute and chronic stages (Fig. 2). Our prior study in this r-mTBI model with C57BL/6 mice showed sparse APP immunolabeling of damaged axons at 6 weeks [90]. Therefore, for the 6-week and 4-month survival time points, we chose SMI-34 immunolabeling (Fig. 2), which is advantageous for detecting axon loss and damage during subacute and chronic stages [30, 53, 78]. In healthy brain, neurofilaments are predominantly non-phosphorylated in neuronal cell bodies and dendrites, in contrast to the phosphorylated neurofilaments of axons [75]. SMI-34 immunolabeling of phosphorylated neurofilament heavy chain (NF200) detected beading and end bulb formation in damaged cortical axons, along with evidence of accumulated phosphorylated neurofilaments in cortical neuron cell bodies (Fig. 2e–g). Axons in the corpus callosum were well labeled by SMI-34 in homozygous mice at 4 months after the sham surgical procedure (Fig. 2h). However, at 4 months post-injury both s-TBI and r-mTBI homozygous mice (Fig. 2i, j) had variable, mottled SMI-34 immunolabeling in the corpus callosum that may indicate axon loss or dephosphorylation,

which is associated with neurofilament compaction in damaged axons [78, 80].

The hang time test that demonstrated deficits with age and genotype in non-injured (naïve) mice (Fig. 1) revealed that neurologic impairment was not accelerated significantly after injury as compared to the sham procedure in mice of each genotype (Fig. 2k–m). Mice were tested weekly out to 4 months post-injury. In wild-type mice, neither r-mTBI nor r-sham resulted in hang time deficits (Fig. 2k). A minority of hemizygous mice exhibited hang time deficits beginning at 2 months post-injury (Fig. 2l). The majority of homozygous mice developed progressive hang time impairments but this was not a specific injury effect since the decline was similar after r-mTBI and r-sham procedures (Fig. 2m).

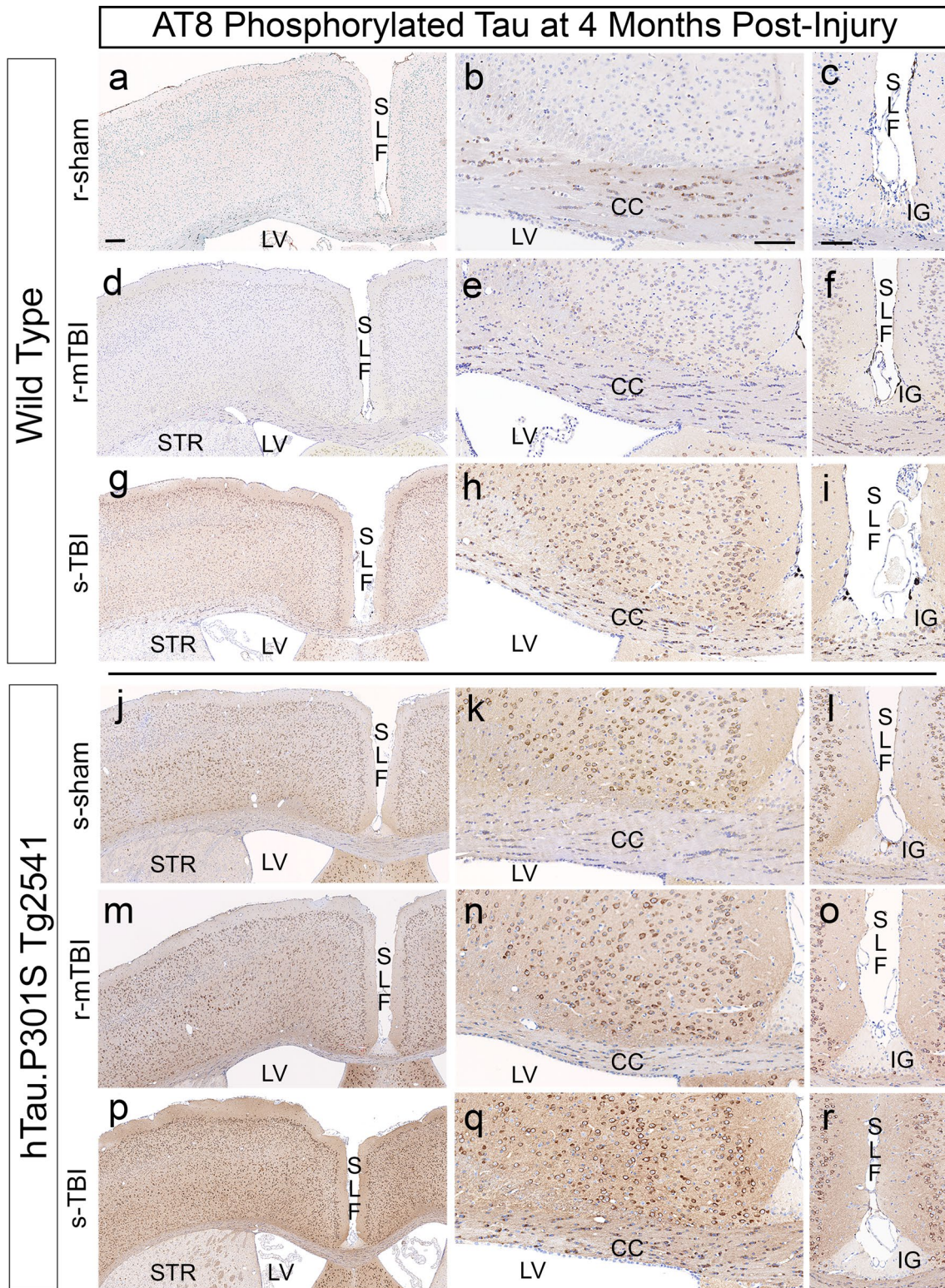
Chronic-stage phosphorylated tau neuropathology varies with head injury conditions and hTau.P301S genotype

We next evaluated tau pathology in coronal brain sections at the chronic stage of 4 months after s-TBI or r-mTBI, and corresponding sham conditions, and found injury induced phosphorylated tau in wild-type mice that was amplified in homozygous mice. The initial characterization of the hTau.P301S Tg2541 line tested a battery of antibodies and reported that AT8 detected tau phosphorylation in the largest number of cells [2]. Therefore, we evaluated AT8 immunolabeling in medial cerebral cortex and corpus callosum regions under the impact site (Fig. 3 and Table 2).

In wild-type mice, coronal brain sections show increasing AT8 immunolabeling in cells under the impact site with increasing injury severity (Fig. 3a–i). This increase was most evident in the medial cerebral cortex, particularly in the superficial cortical layers, after the moderate s-TBI (Fig. 3g). Sham mice exhibit little AT8 in cortical neurons while strong AT8 immunolabeling was present in the cytoplasm of cells with the morphology of oligodendrocytes in the corpus callosum (Fig. 3b).

In homozygous mice, strong AT8 immunolabeling was found in cortical neurons in sham and injured mice (Fig. 3j–r). The intensity of AT8 immunoreactivity in the medial cortex appeared to increase with injury severity to be most pronounced after the s-TBI (Fig. 3p). After s-TBI, AT8 immunolabeling of neuronal processes was also notable across cortical layers and in the corpus callosum (Fig. 3q).

The superior longitudinal fissure region was also examined as potentially analogous to human cortical sulci, which are sites of AT8 accumulation in cases of CTE [19, 45]. In wild-type and homozygous mice, labeled cells were present along the pial surface in the fissure (Fig. 3). Rare AT8 immunolabeled cells were also present in the depth of the fissure along the vasculature or the junction of the gray matter over the corpus callosum (Fig. 3l, o, r).



Interestingly, the region of the indusium griseum is not immunolabeled with AT8, which supports the specificity of the AT8 signal in cortical neuron processes in the adjacent tissue (Fig. 3l, o, r). The indusium griseum is a band

of non-cortical cells that runs rostro-caudally superior to the corpus callosum in human brain [13] and rostral mouse brain [1], which may limit comparison of the rostral superior longitudinal fissure to human cortical sulci.

Fig. 3 AT8 detection of phosphorylated tau pathology varies with injury conditions and hTau.P301S genotype at 4 months after TBI or sham procedures. **a–c** Sham wild-type mice do not exhibit AT8 immunolabeling of cortical neurons. In contrast, strong AT8 immunolabeling is found in oligodendrocytes in the corpus callosum (CC). **d–f** Wild-type r-mTBI mice exhibit AT8 in the cytoplasm of oligodendrocytes, which typically appear as small round cells that are aligned in rows within the CC and sparsely distributed in cortical regions. **g–i** Wild-type s-TBI mice exhibit clear AT8 immunolabeling in cortical neurons, particularly in superficial layers, along with CC thinning. **j–l** In homozygous sham mice, AT8 immunolabels cortical neurons and callosal oligodendrocytes. **m–o** Homozygous r-mTBI mice exhibit cortical AT8 immunolabeling, along with CC thinning. **p–r** Homozygous s-TBI mice exhibit strong cortical AT8 immunolabeling, along with CC thinning. **a–r** Nuclei stained blue with hematoxylin. Scale bars: left column shown in $a=200\ \mu\text{m}$; middle column in $b=100\ \mu\text{m}$, right column in $d=100\ \mu\text{m}$. Abbreviations: Superior longitudinal fissure (SLF), lateral ventricle (LV), corpus callosum (CC), striatum (STR), indusium griseum (IG)

Endogenous mouse tau is phosphorylated in cortical neurons during chronic phase TBI in wild-type mice

Further analysis of AT8 immunolabeling confirmed endogenous mouse tau phosphorylation in cortical neurons of wild-type mice at 4 months after s-TBI (Fig. 4a–d). HT7 immunolabeling is specific for human tau and does not recognize endogenous mouse tau. After s-TBI in wild-type mice, cortical neurons were clearly immunolabeled with AT8, in the absence of HT7 immunolabeling (Fig. 4a, b). In contrast, after s-TBI in homozygous mice, cortical neurons were strongly immunolabeled for AT8 with corresponding HT7 immunolabeling (Fig. 4c, d). HT7 immunostaining was present in neurons across cortical layers 2–6 (Fig. 4d), as expected from the Thy1.2 neuronal promoter [23].

Phosphorylated Tau is localized in axons during chronic phase TBI in tau homozygous mice

In addition to AT8 immunolabeling of cortical neuron cell bodies, axons were also clearly immunolabeled with AT8 in injured homozygous mice at 4 months after s-TBI (Fig. 5). Cortical neurons of the medial cerebral cortex (anterior cingulate cortex, motor cortex) project axons through the corpus callosum that descend in bundles within the striatum [17, 25]. In agreement with this pathway, AT8 immunolabeling of axons was evident in fibers within the corpus callosum (Fig. 5a, b) and descending through the striatum (Fig. 5e, f) in Tg2541 homozygous s-TBI mice. Striatal neurons lacked AT8 immunolabeling (Fig. 5a, e), even in the presence of human tau transgene expression (Fig. 5b, f). AT8 immunoreactivity was not evident in axons of the corpus callosum (Fig. 5c, d) or striatum (Fig. 5g, h) in absence of injury in wild-type mice.

Analysis of AT8 in comparison to HT7 in the corpus callosum and striatum also revealed striking AT8 immunolabeling of endogenous mouse phosphorylated tau in the cytoplasm of oligodendrocytes (Fig. 5). AT8 immunolabeled oligodendrocytes in wild-type mice with only the sham procedure (Fig. 5c, g). Therefore, oligodendrocytes did not require injury or mutant tau expression to exhibit tau phosphorylation. Oligodendrocytes were not immunolabeled with HT7 in homozygous mice, indicating that AT8 immunolabeling in oligodendrocytes was detecting endogenous mouse tau (Fig. 5b, f). This result is in agreement with reports of cytoplasmic tau expression in oligodendrocytes in normal adult mice [48, 79] and after TBI [37].

Multiple phospho-tau epitopes are increased in brain lysates of tau transgenic mice

Quantitative analysis of brain lysates demonstrated significant increases of total human mutant tau and specific phosphorylated tau epitopes in Tg2541 transgenic mice (Fig. 6). Brain lysates were prepared from bilateral regions under the impact site (Fig. 6a). This dissection captures corpus callosum axons along with the corresponding callosal projection neurons [91] to account for potential phosphorylation dependent redistribution of tau from the axon resulting in mis-localization in the somatodendritic compartment [39]. These brain regions under the impact site have shown axon damage after s-TBI and r-mTBI in Thy1-YFP-16 mice in our prior studies [54] [90]. Soluble proteins were isolated and probed for tau epitopes using Wes Protein Simple capillary electrophoresis immunoassays (Fig. 6b). Soluble tau was quantified as an early stage of phosphorylated tau that is relevant to the axonal compartment and the response to traumatic injury. Soluble tau can disrupt axonal transport and have detrimental effects independent of plaques and tangles [18, 70].

Soluble human tau protein was recognized with the HT7 antibody in wild-type, hemizygous, and homozygous Tg2541 mice after s-TBI (Fig. 6c–f) or r-mTBI (Fig. 6g–j). HT7 did not detect wild-type mouse tau when run with the same protein loading and antibody dilution as the transgenic mice (Fig. 6c, g). Phosphorylated tau epitopes (pT205, pT231, pS404) were markedly increased in transgenic mice. Wild-type mice also exhibited phosphorylation of endogenous mouse tau for T205, which is one of two tau epitopes recognized by AT8, and for S404, which is associated with axonal tau. Across genotypes, soluble tau and phospho-tau levels were not altered by s-TBI or r-mTBI, as compared to the respective sham procedures in mice of each genotype.

Table 2 Localization of phosphorylated tau pathology in coronal sections under the impact site

Injury	hTau	Corpus callosum		Deep CTX layers IV–VI	Sites relevant to chronic traumatic encephalopathy					
		Cells	Axons		Superficial CTX		SL fissure depth		CTX peri-vascular cells	Peri-ventricular
					Pial or subpial (I)	Layers II/III	Peri-vascular	Layer I		
s-sham	WT	++	–	+	+	+	±	+	–	–
s-TBI	WT	++	+	++	++	+++	+	+	±	+
r-sham	WT	++	–	±	+	+	+	±	–	–
r-mTBI	WT	+	–	±	+	+	++	–	±	±
s-sham	Hom	+	+	++	+	++	+	+	+	+
s-TBI	Hom	++	++	+++	+++	++++	+	+	+	+
r-sham	Hom	+	+	+++	+++	+++	+	++	±	+
r-mTBI	Hom	+	+	+++	+++	+++	++	+	+	+

Roman numerals designate layers of cerebral cortex

Note: Thy1.2 promoter in Thy1-YFP-16 mice labels neurons in cortical layers II–VI (Feng et al. 2000)

CTX cerebral cortex, SL superior longitudinal

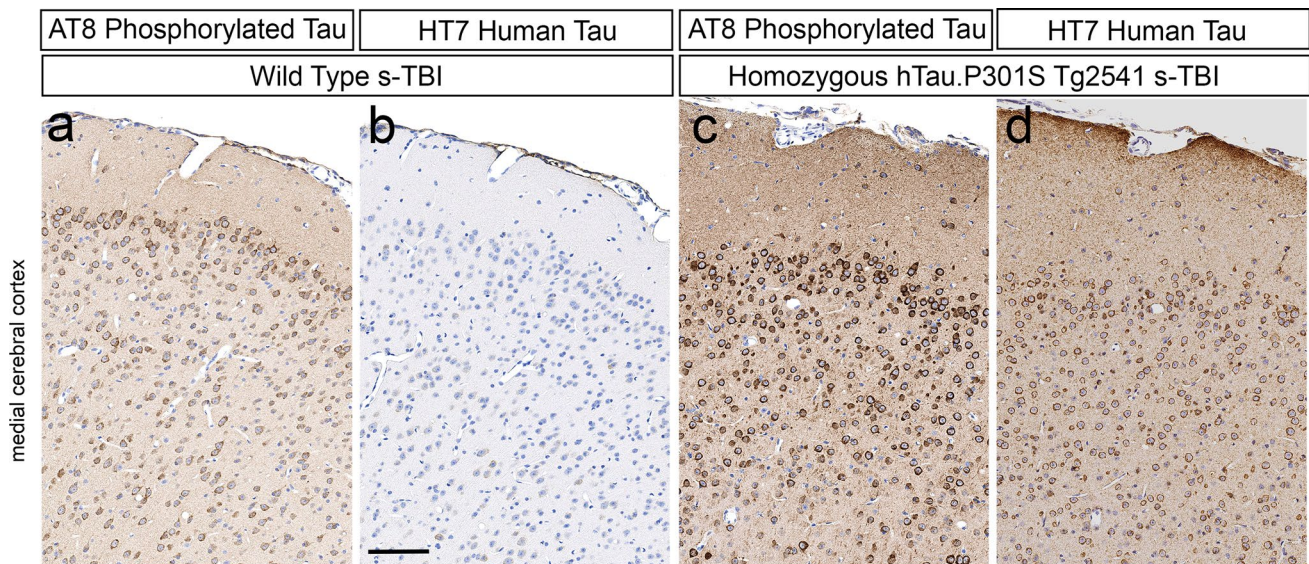


Fig. 4 Demonstration of endogenous mouse tau phosphorylation in cortical neurons at 4 months after s-TBI in comparison with human tau expression. **a, b** After s-TBI in wild-type mice, cortical neurons exhibit clear AT8 immunolabeling of phosphorylated endogenous

mouse tau, which is not labeled with the HT7 antibody. **c, d** After s-TBI in homozygous mice, cortical neurons exhibit strong AT8 immunolabeling and HT7 detection of human tau. **a–d** Nuclei stained blue with hematoxylin. Scale bars for **a–d** shown in **B** = 200 μ m

Chronic white matter pathology is significantly worsened in tau homozygous mice after TBI

In contrast to prior mouse TBI studies [5, 27, 58], we found significant effects of human tau transgene expression on the progression of white matter pathology between subacute to chronic time points post-injury (Figs. 7, 8, 9, 10). Corpus callosum width and myelination measures were used as indicators of post-traumatic neurodegeneration after s-TBI and r-mTBI. Mice of each tau genotype were compared at

6 weeks and 4 months post-injury to assess the progression of white matter pathology at subacute and chronic stages, respectively.

A striking difference was observed for the effect of tau genotype on corpus callosum width between injury models. Coronal sections of regions under the impact site were examined with hematoxylin and eosin histological stain, which is widely used for clinical and experimental neuropathology (Figs. 7, 8). After s-TBI, the corpus callosum width was significantly reduced at both 6 weeks and 4 months post-injury,

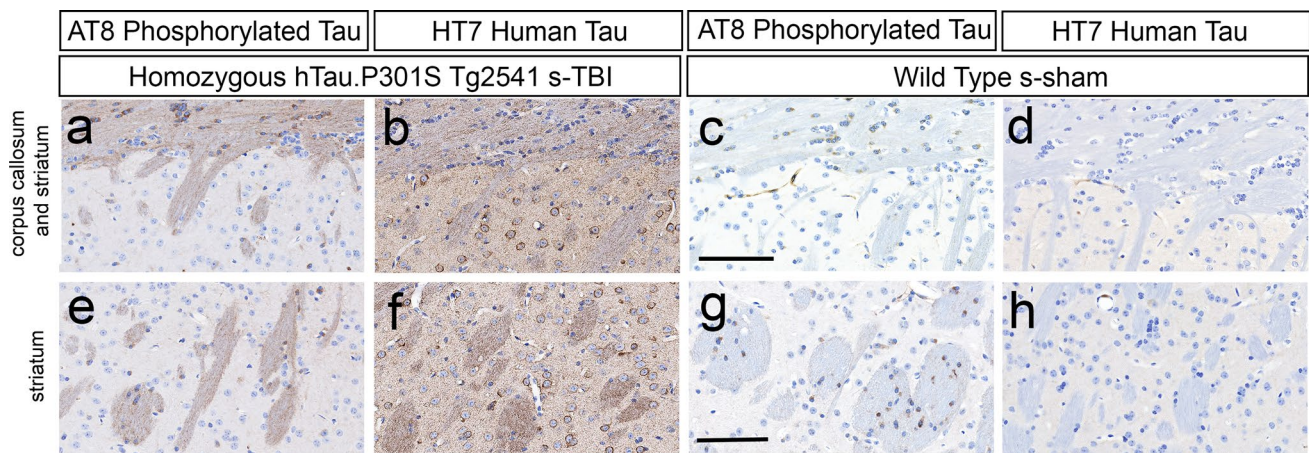


Fig. 5 Tau phosphorylation in axons and oligodendrocytes. **a, b** After s-TBI in homozygous mice, AT8 immunolabels axons and small round oligodendrocytes in the CC. Striatal neurons underlying the CC are not immunolabeled with AT8, but do express the human transgene as detected with the HT7 antibody. **c, d** In sham wild-type mice, AT8 labels oligodendrocytes in the CC and underlying striatum. A lack of HT7 signal confirms that the oligodendrocyte AT8 signal reflects endogenous mouse tau phosphorylation. **e, f** After s-TBI

in homozygous mice, deeper striatal regions show AT8 immunolabeling of cortical neuron axon bundles and small round oligodendrocytes. The neurons are not immunolabeled with AT8, but do express the human transgene as detected with HT7. **g, h** In sham wild-type mice, deeper striatal regions show distinct AT8 immunolabeling of oligodendrocytes near axon bundles, in the absence of HT7 immunostaining. **a–h** Nuclei stained blue with hematoxylin. Scale bars: **a–d** shown in $c = 100 \mu\text{m}$, **e–h** in $g = 100 \mu\text{m}$

as compared to sham controls (Fig. 7e, f). Tau genotype did not have a significant effect on the corpus callosum width after s-TBI (Fig. 7e, f). In contrast, the r-mTBI model did not reduce corpus callosum width at 6 weeks post-injury, as compared to the sham procedure, in mice of any of the three genotypes (Fig. 8e). At 4 months after r-mTBI, the corpus callosum thinning was still not observed in wild-type or hemizygous mice (Fig. 8f). Importantly, in tau homozygous mice, significant worsening of corpus callosum thinning developed by 4 months after r-mTBI (Fig. 8f). Therefore, the repetitive mild closed head injury in mice with high tau pathology resulted in a delayed progression of white matter injury that produced dramatic corpus callosum atrophy.

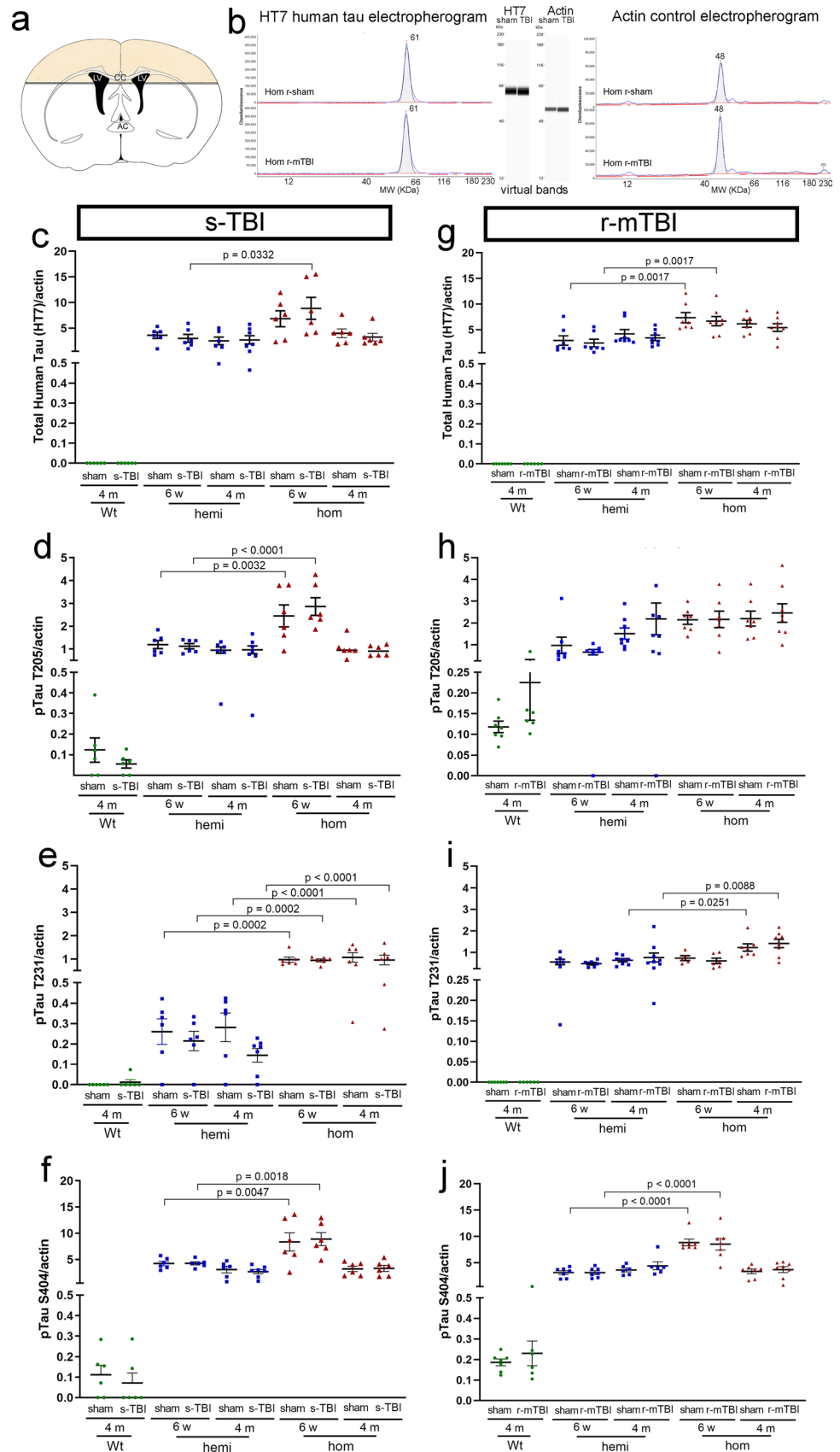
Analysis of myelination, with immunolabeling for myelin basic protein (MBP), corroborated the chronic-stage effect of tau genotype from the histological stain in r-mTBI mice and revealed an additional late demyelination effect in the s-TBI model (Figs. 9, 10). The delayed corpus callosum thinning after r-mTBI was found only in tau homozygous mice (Fig. 9e), matching the findings shown in Fig. 8f. The r-mTBI mice did not show significant corpus callosum or cortical demyelination, i.e., loss of myelin staining, across genotypes (Fig. 9f, g). After s-TBI, the injury had a significant effect of reduced corpus callosum width that was similar across genotypes (Fig. 10e), as in Fig. 7f. In addition to this persistent corpus callosum atrophy after s-TBI, significant demyelination developed between the subacute and chronic time points in the corpus callosum and cortex that was found only in the tau homozygous mice (Fig. 10f, g). These results indicate that homozygous mutant tau transgene

expression worsened the progression of white matter pathology in both r-mTBI and s-TBI models. The comparison of Wt and hom mice in each injury model demonstrates a large effect size of increased tau in addition to the significant p value determination. The chronic-stage onset of corpus callosum atrophy after r-mTBI has a Cohen's $d = 2.16$ and the additional pathology of demyelination with atrophy after s-TBI has a Cohen's $d = 2.91$, indicating that the hom are more than 98% below the Wt values for each finding.

Both s-TBI and r-mTBI injuries increase microgliosis in the corpus callosum that is enhanced in tau homozygous mice

Neuroinflammation, particularly a chronic microglial response, may contribute to the worsening of chronic-stage white matter pathology that was identified with increased tau pathology. Both s-TBI and r-mTBI induced reactive microglia (Fig. 11) and astrocytes (Fig. 12) in the corpus callosum. The corpus callosum microglial response was significantly increased with tau in homozygous mice after both s-TBI and r-mTBI at the subacute phase and persisted during the chronic phase (Fig. 11g–j). The microglial and astrocytic response was more prominent in the white matter than in the adjacent medial cortex under the impact site (Fig. SI-5; Tables SI-6 and SI-7). The astrocyte response was not increased in tau homozygous mice (Fig. 12g–j). In addition, after r-mTBI, the astrocyte reaction was only significant at the subacute time point and had resolved by the chronic phase (Fig. 12j). These results indicate that microgliosis

Fig. 6 Total human tau and phosphorylated tau are increased in brain lysates of tau transgenic mice. **a** Brain lysates were prepared from the colored cortical regions and white matter tracts, including the corpus callosum (CC) over the lateral ventricles (LV). This superior brain region was dissected from a 2-mm thick coronal slice to capture cortical neuron cell bodies and corresponding axons. **b** Tau epitopes were quantified in the soluble fraction from brain lysates using Protein Simple Wes capillary electrophoresis immunoassay with actin for normalization of the protein loading amounts. The automated quantification is displayed as electropherograms with the same data also displayed as virtual bands in a blot-like image. **c–j** The HT7 antibody recognizes total human tau to detect the human transgene expression. In contrast, the antibodies to phosphorylated tau epitopes recognize both human and mouse epitopes. Dots represent individual mice with wild type (Wt) in green, hemizygous (hemi) in blue, and homozygous (hom) in red. Non-significant comparisons are not shown. See Supplemental Information for full statistical analysis provided in Table SI-8, which includes analysis showing a general lack of sex differences. **c–f** Comparison across genotypes for s-TBI and s-sham mice at 6 weeks and 4 months post-injury. **g–j** Comparison across genotypes for r-mTBI and r-sham mice at 6 weeks and 4 months post-injury



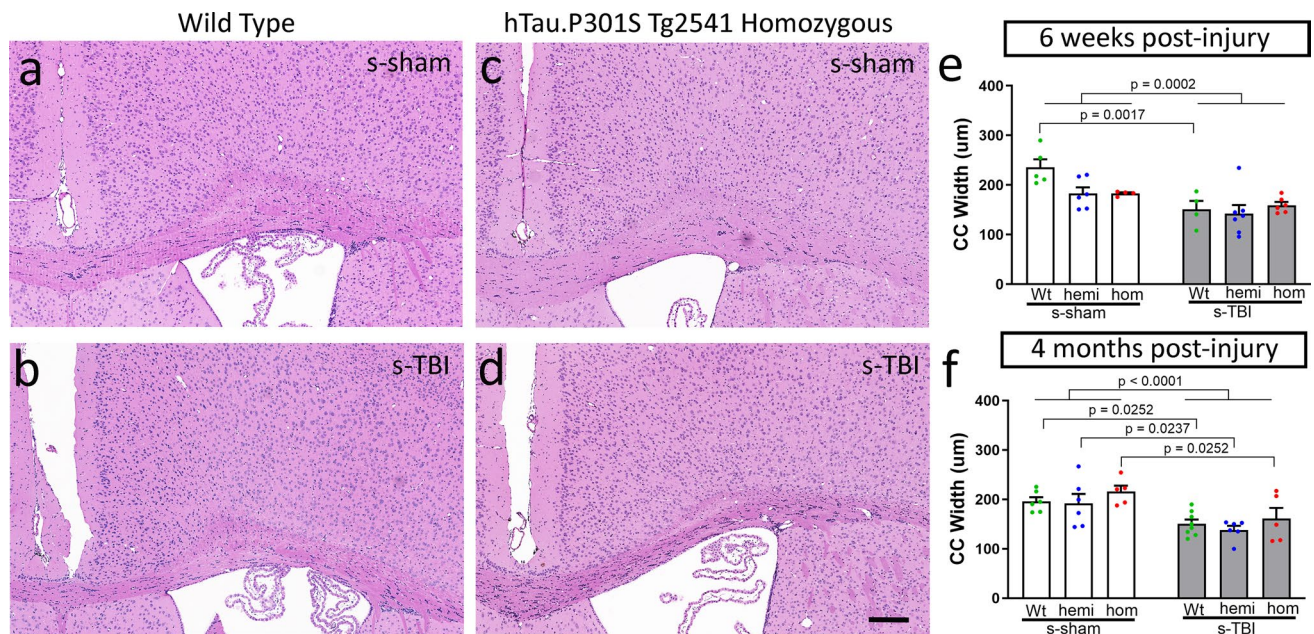


Fig. 7 Moderate s-TBI produces corpus callosum atrophy that is not altered by tau genotype. **a–d** Coronal sections through the medial cortex and corpus callosum under the impact site with cell nuclei stained with hematoxylin (blue) and cytoplasm with eosin (pink). Corpus callosum thinning is evident at 4 months post-injury after s-TBI, as compared to sham, in wild-type (**a, b**) and tau homozygous mice (**c, d**). Scale bars for **a–d** shown in **d** = 200 μm . **e** Corpus callosum width is reduced due to a main effect of injury at the subacute

phase. **f** Corpus callosum width is significantly reduced due to injury in s-TBI versus sham conditions for each genotype at the chronic phase. Tau genotype does not worsen corpus callosum thinning. **e, f** Dots represent individual mice with wild type (Wt) in green, hemizygous (hemi) in blue, and homozygous (hom) in red. Non-significant comparisons are not shown. See Supplemental Information for full statistical analysis provided in Table SI-6, along with the number and sex of mice for each group

accompanies white matter pathology during the chronic phase post-injury.

Translational blood biomarker assay detects axonal injury and human tau exposure levels

A blood biomarker assay used in clinical TBI research [14, 49, 68] was effective as a translational non-invasive method to monitor axonal injury and tau exposure from mouse serum samples (Fig. 13). The Simoa® Neurology 4-Plex A was used to test for simultaneous analysis of tau, neurofilament (Nf-L), glial fibrillary acidic protein (GFAP), and ubiquitin carboxyl-terminal hydrolase L1 (UCH-L1) in a given mouse serum sample. This clinical assay effectively detected human tau expressed from the hTau.P301S transgene that continued to be present at high levels in serum of homozygous mice across acute (1 day), subacute (6 weeks), and chronic (4 months) time points (Fig. 13a–f). The Neurology 4-Plex A detects mouse Nf-L with specificity, a demonstrated by signal elimination with immunodepletion, but is not likely to have the appropriate specificity to detect mouse GFAP or mouse UCH-L1 (see “Methods”), in agreement with our results (data not shown). Nf-L levels were sensitive to axon damage that reflected the injury effect at the acute phase (Fig. 13g, j). With progression to the chronic phase, Nf-L

levels were dramatically elevated in homozygous mice relative to wild-type for s-sham (41.4-fold), s-TBI (45.6-fold), r-sham (32.3-fold) and r-mTBI (49.2-fold) mice. This elevated serum Nf-L level indicates prolonged axon degeneration with continued human mutant tau expression (Fig. 13i, l). Both the s-TBI and the r-mTBI produced similar findings for human tau and mouse Nf-L biomarker profiles.

Discussion

The main finding of this study is that increasing pathological tau worsens white matter degeneration after TBI, which is most notable as delayed, chronic phase corpus callosum atrophy after repetitive mild TBI. Demonstrating this interplay over time between tau pathology and long-term outcomes after TBI is challenging in post-mortem human specimens and has remained elusive in animal models. However, a recent study in wild-type mice using a closed head injury model similar to our r-mTBI, and supported with a systematic review of the literature in wild-type strains, demonstrated the suitability of mouse TBI models to replicate pertinent human tau histopathology [45]. Yet, two recent experimental studies and a systematic review of TBI in mouse strains expressing human tau

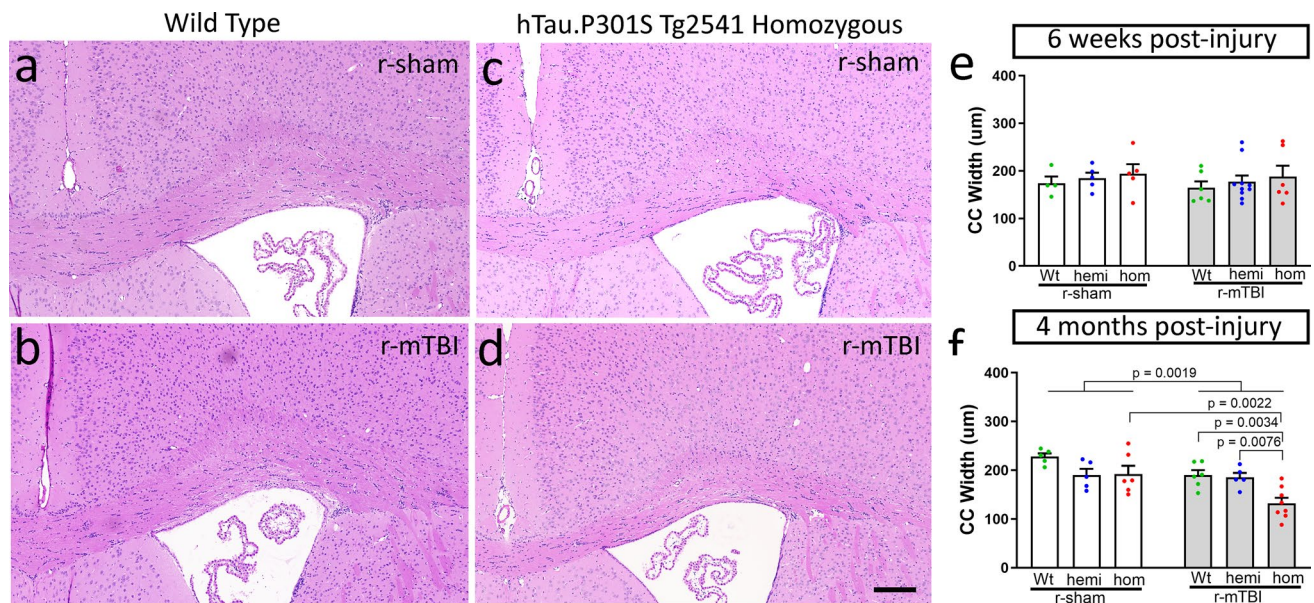


Fig. 8 Increased pathological tau produces delayed corpus callosum atrophy in chronic r-mTBI. **a–d** Coronal sections through the medial cortex and corpus callosum under the impact site with cell nuclei stained with hematoxylin (blue) and cytoplasm with eosin (pink). Normal adult corpus callosum thickness is seen in wild-type mice, both sham (**a**) and injured (**b**), and in sham tau homozygous mice (**c**) at the 4-month time point. Corpus callosum thinning is evident at 4 months post-injury after r-mTBI only in homozygous tau mice (**d**). Scale bars for **a–d** shown in **d** = 200 µm. **e** Corpus callosum width is

not altered by r-mTBI or tau genotype at the subacute phase. **f** The r-mTBI results in a dramatic reduction of corpus callosum width by the chronic phase only when combined with the homozygous tau genotype, but not in wild-type and hemizygous mice. **e, f** Dots represent individual mice with wild type (Wt) in green, hemizygous (hemi) in blue, and homozygous (hom) in red. Non-significant comparisons are not shown. See Supplemental Information for full statistical analysis provided in Table SI-7 along with the number and sex of mice for each group

constructs did not identify a direct link between elevated phosphorylated tau after TBI and worsened functional outcome and did not find evidence of a role of tau in neuropathological sequelae after TBI [5, 58].

Our results reveal a complex interplay of increasing pathological human tau relative to the extent of white matter injury and a delayed progression of pathology between the subacute to a chronic stage. We bred mice of the hTau.P301S (Tg2541) strain to increase phosphorylated tau pathology in relevant neuron and axon populations to evaluate the effects of 0, 1, or 2 human mutant tau alleles. In the context of a low level of axon damage in the r-mTBI model, increased pathological tau in homozygous mice resulted in significant progression of corpus callosum atrophy between the subacute (6 weeks) to chronic (4 months) time points (Figs. 8e, f, 9e). In the moderate s-TBI model, which produces more extensive axonal damage in the corpus callosum, corpus callosum atrophy began in the subacute phase and persisted at chronic time points, regardless of tau genotypes (Figs. 7e, f, 10e). Still, the combination of s-TBI with increased tau in homozygous mice worsened pathology of myelinated axons between the subacute and chronic phases based on our findings of late demyelination in the corpus callosum (Fig. 10f). Interestingly, the homozygous genotype increased the microglial

response to injury at both the subacute and chronic phase in both s-TBI and r-mTBI models (Fig. 11).

The P301S human tau mutation was chosen for the current studies as an effective means of increasing phosphorylated tau pathology to inform interpretation of neuropathological sequelae in human TBI cases. These results also support a role of TBI as a modifiable risk factor in frontotemporal dementia (FTD). The human P301S tau mutation, which is expressed in the Tg2541 transgenic mice, is found in early onset FTD [2, 88]. Among FTD patients, suffering a TBI was associated with early onset and sporadic FTD [46, 74]. The interplay of tau pathology and TBI emphasizes the need to identify the direct and/or indirect mechanism(s) by which TBI pathophysiology initiates tau phosphorylation in axons and the subsequent tau pathology, which remain areas of intense research.

The contribution of traumatic axonal injury in white matter atrophy, as demonstrated in our prior studies in *Sarm1* null mice, further supports an interplay of neuronal tau pathology and TBI in our current results. Deletion of the *Sarm1* gene inactivates the SARM1 pathway that executes a highly conserved molecular process of axon degeneration [24, 67]. Acute axonal degeneration at 3 days after s-TBI is dramatically reduced in *Sarm1* null mice as compared to wild-type mice [53]. During the chronic phase at 10 weeks

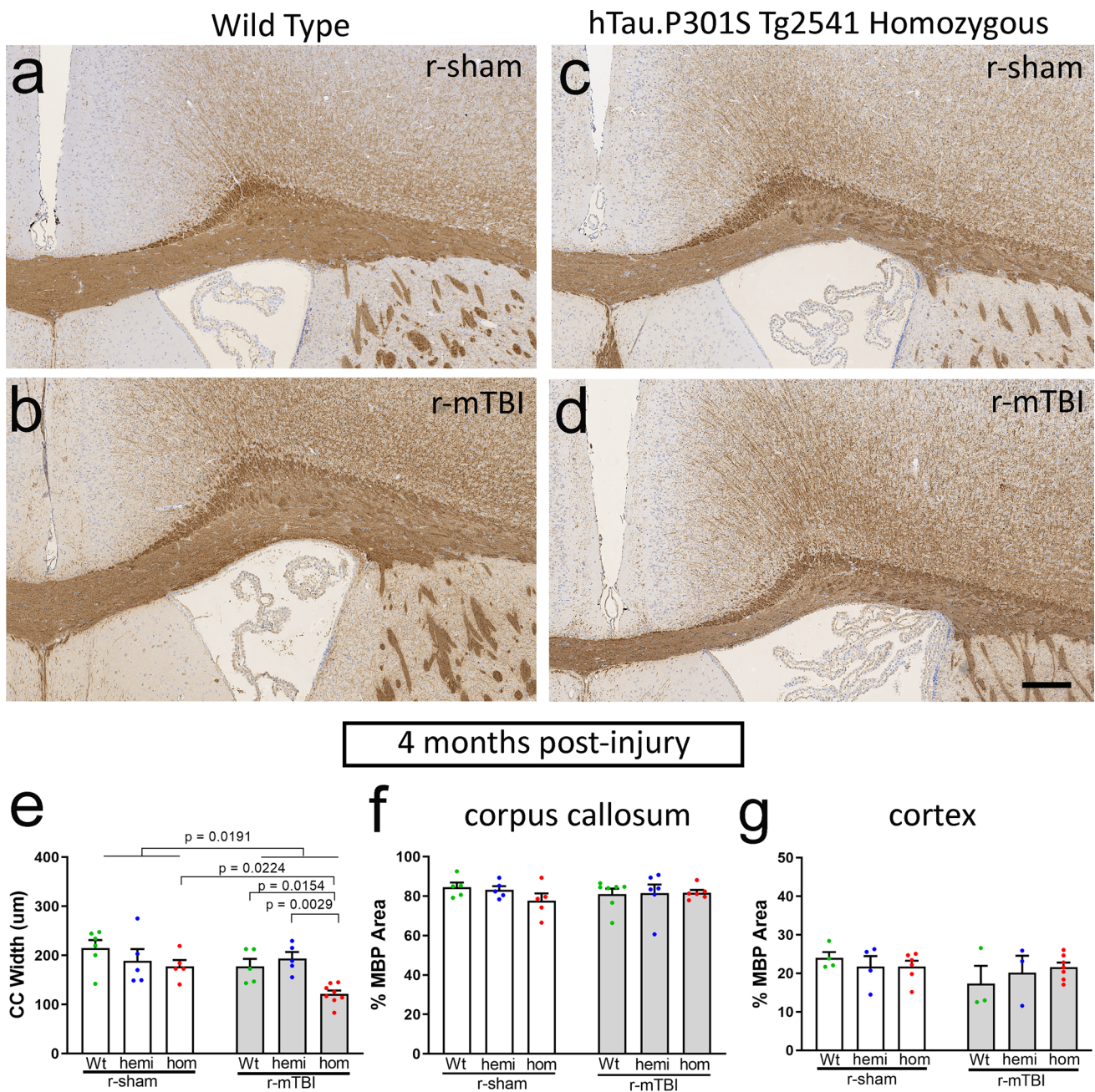


Fig. 9 Myelin immunolabeling corroborates delayed corpus callosum atrophy with increased pathological tau in chronic r-mTBI. **a–d** Coronal sections through the medial cortex and corpus callosum under the impact site with myelin labeled by immunohistochemistry for myelin basic protein (MBP). Nuclei stained blue with hematoxylin. Normal adult corpus callosum thickness is seen in wild-type mice, both sham (**a**) and injured (**b**), and in sham tau homozygous mice (**c**) at the 4-month time point. Corpus callosum thinning is evident at 4 months post-injury after r-mTBI only in homozygous tau mice (**d**). Scale bars for **a–d** shown in $D=200\ \mu\text{m}$. **e** The r-mTBI results in a dramatic

reduction of corpus callosum width by the chronic phase only when combined with the homozygous tau genotype, but not in wild-type and hemizygous mice. **f, g** The r-mTBI did not cause loss of myelinated areas within the corpus callosum (**f**) or overlying cortex (**g**) across genotypes. **e–g** Dots represent individual mice with wild type (Wt) in green, hemizygous (hemi) in blue, and homozygous (hom) in red. Non-significant comparisons are not shown. See Supplemental Information for full statistical analysis provided in Table SI-7, along with the number and sex of mice in each group

after s-TBI, *Sarm1* null mice have both reduced axon degeneration and reduced corpus callosum atrophy [10]. The s-TBI model produced more axon damage in the corpus callosum

than r-mTBI (Fig. 1d, e, SI-3), and developed corpus callosum atrophy at an earlier time post-injury. Both models use the same impact location (bregma coordinates) and

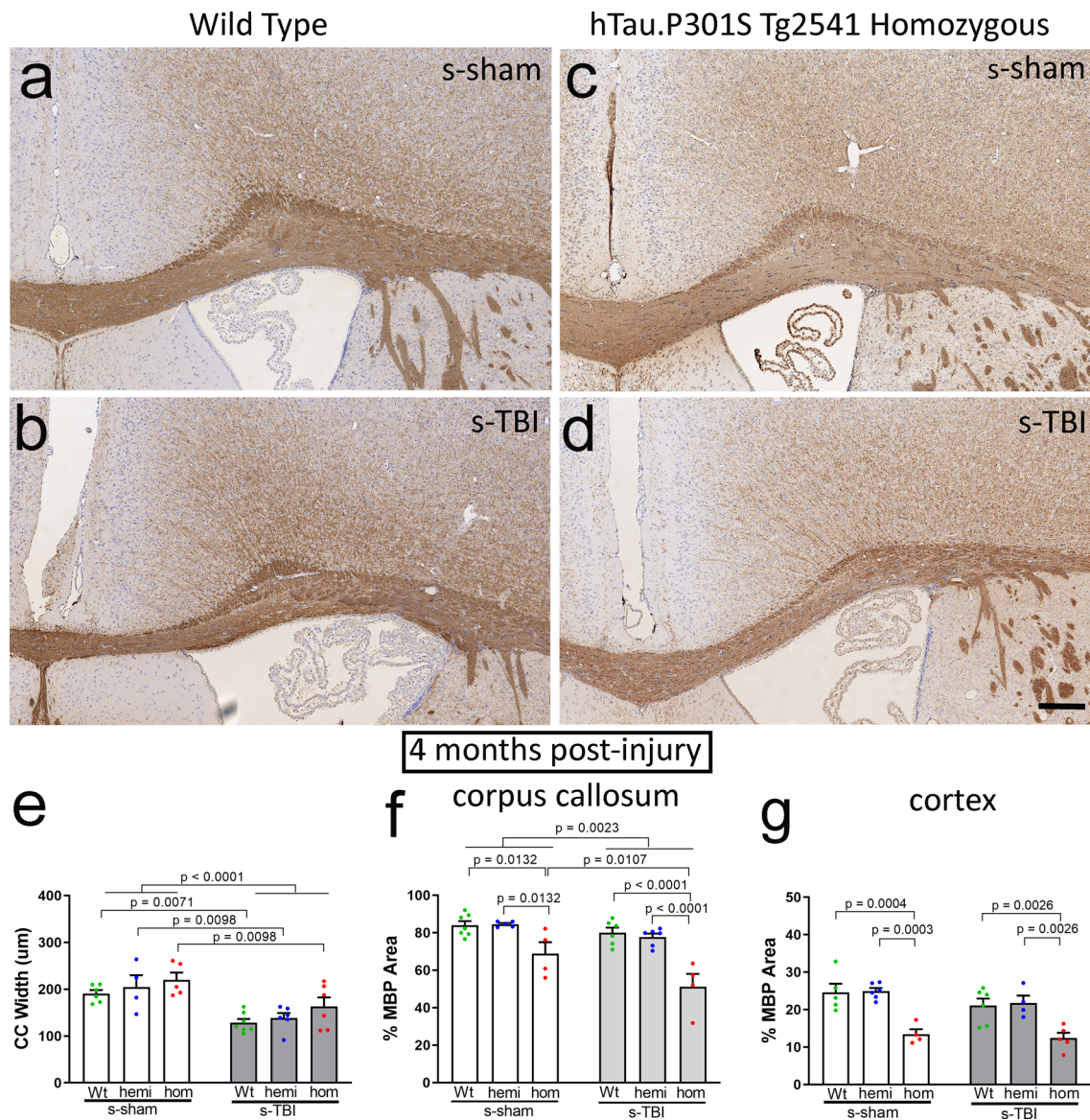


Fig. 10 Myelin immunolabeling shows persistent corpus callosum atrophy after s-TBI, and that increased pathological tau produces late-stage demyelination. **a–d** Coronal sections through the medial cortex and corpus callosum under the impact site with myelin labeled by immunohistochemistry for myelin basic protein (MBP). Nuclei stained blue with hematoxylin. Normal adult corpus callosum thickness is seen in wild-type sham mice (**a**) with thinning after s-TBI (**b**). Similarly, in tau homozygous mice, the corpus callosum is notably thicker in sham mice (**c**) as compared to injured mice at the 4-month time point (**d**). Scale bars for **a–d** shown in **d** = 200 μ m. **e** During chronic phase s-TBI, the corpus callosum width is significantly

reduced across genotypes. **f** Increased tau pathology in homozygous mice results in loss of myelinated areas within the corpus callosum that is present after the s-sham procedure and significantly worsened in combination with s-TBI. **g** Increased tau pathology in homozygous mice results in loss of myelinated areas within the cortex that is similar after s-sham and s-TBI procedures. **e–g** Dots represent individual mice with wild type (Wt) in green, hemizygous (hemi) in blue, and homozygous (hom) in red. Non-significant comparisons are not shown. See Supplemental Information for full statistical analysis provided in Table SI-6, along with the number and sex of mice for each group

velocity (4 mm/s) while differences are based on the impact depth, which is greater for s-TBI (1.5 mm) than for r-mTBI (1.0 mm), and impact being made onto the skull (s-TBI) or onto the scalp to facilitate repetitive impacts (r-mTBI) (Fig. 1b and methods). Our prior studies in C57BL/6 mice [77, 90] using the s-TBI and r-mTBI models showed that

axon damage, as detected by APP detection, decreased between 1 and 7 days post-injury, which supports the current comparison at 1 day after the single or final impact to capture the acute time point and may also be a consideration for interpreting the cumulative effect across the 5-day r-mTBI series.

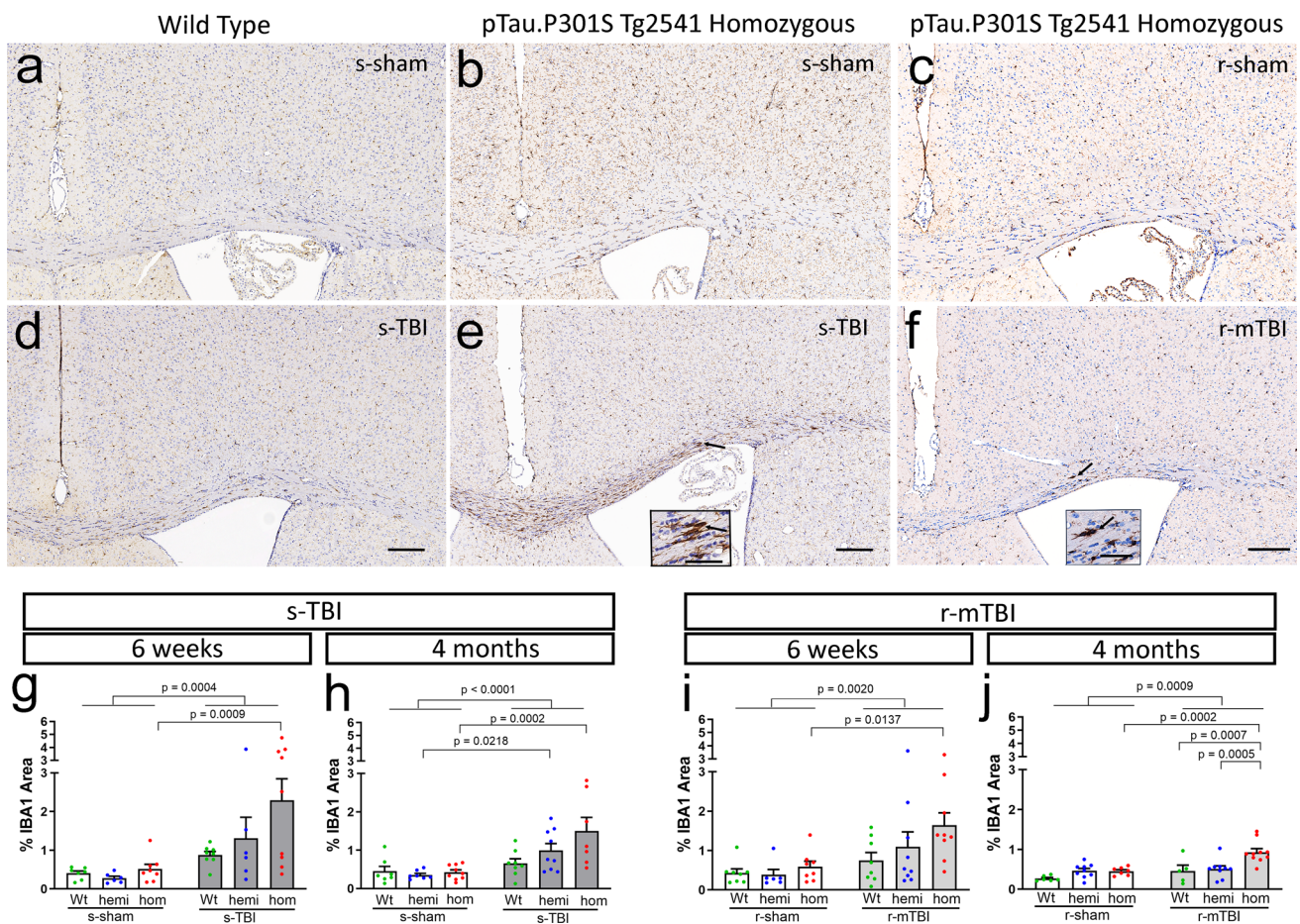


Fig. 11 Both s-TBI and r-mTBI injuries induced a microglial response in the corpus callosum that was most prominent in tau homozygous mice. **a–f** Immunohistochemistry for IBA1 to identify microglia in coronal sections under the impact site. Nuclei stained blue with hematoxylin. Images shown are 4 months post-injury or sham procedures. Scale bars inset 50 μ m, panel images 200 μ m. **a–c** The microglia appeared similar in the cortex and corpus callosum of sham wild-type (**a**) and tau homozygous mice (**b**, **c**). **d–f** Both s-TBI (**d**, **e**) and r-mTBI (**f**) appeared to increase IBA1 immunolabeling of microglia in the corpus callosum, with prominent enlargement and elongation after s-TBI in homozygous mice (**e**). **g–j** Quantifica-

tion of IBA1 immunolabeling in the corpus callosum shows that the tau homozygous genotype is associated with a significant response to injury at both injury models and at both post-injury time points. Corresponding quantification of IBA1 immunolabeling in the cortex under the impact site is shown in Supplemental Information Fig. SI-5. Dots represent individual mice with wild type (Wt) in green, hemizygous (hemi) in blue, and homozygous (hom) in red. Non-significant comparisons are not shown. See Supplemental Information for full statistical analysis provided in Tables SI-6, SI-7, along with analysis of sex differences which shows that homozygous females have higher IBA1 in the corpus callosum at 6 weeks after s-TBI

White matter atrophy, demyelination, and neuroinflammation develop after TBI in wild-type mice, yet our results show a significant impact of phosphorylated tau pathology on each of these pathological features in the progression from the subacute to chronic phase (Figs. 7, 8, 9, 10, 11, 12). In the s-TBI model, we have shown persistent axon damage and corpus callosum atrophy by neuropathology and MRI fractional anisotropy with volume analysis at 8 and 10 weeks post-injury [10, 54]. Longer term analyses in wild-type mice reported similar findings with different single and repetitive models. White matter atrophy progressed from proximate to remote sites after a single TBI without detectable phosphorylated tau pathology in neurons [37]. Repetitive mild

TBI resulted in corpus callosum atrophy, neuroinflammation and behavioral deficits with longer post-injury intervals of 6 and 12 months [59]. In addition, corpus callosum atrophy and reduced fractional anisotropy were found at 6 and 12 months after repetitive mild TBI, and increased plasma neurofilament light levels at one week after repetitive mild TBI correlated with corpus callosum atrophy on MRI at 12 months [57].

Neuropathologically, demyelination is classically identified as a decrease in the area or density of myelin staining [76], as in our finding of reduced myelin staining in the corpus callosum at 4 months after s-TBI months in homozygous mice (Fig. 10f). This loss of myelin stain may reflect a loss

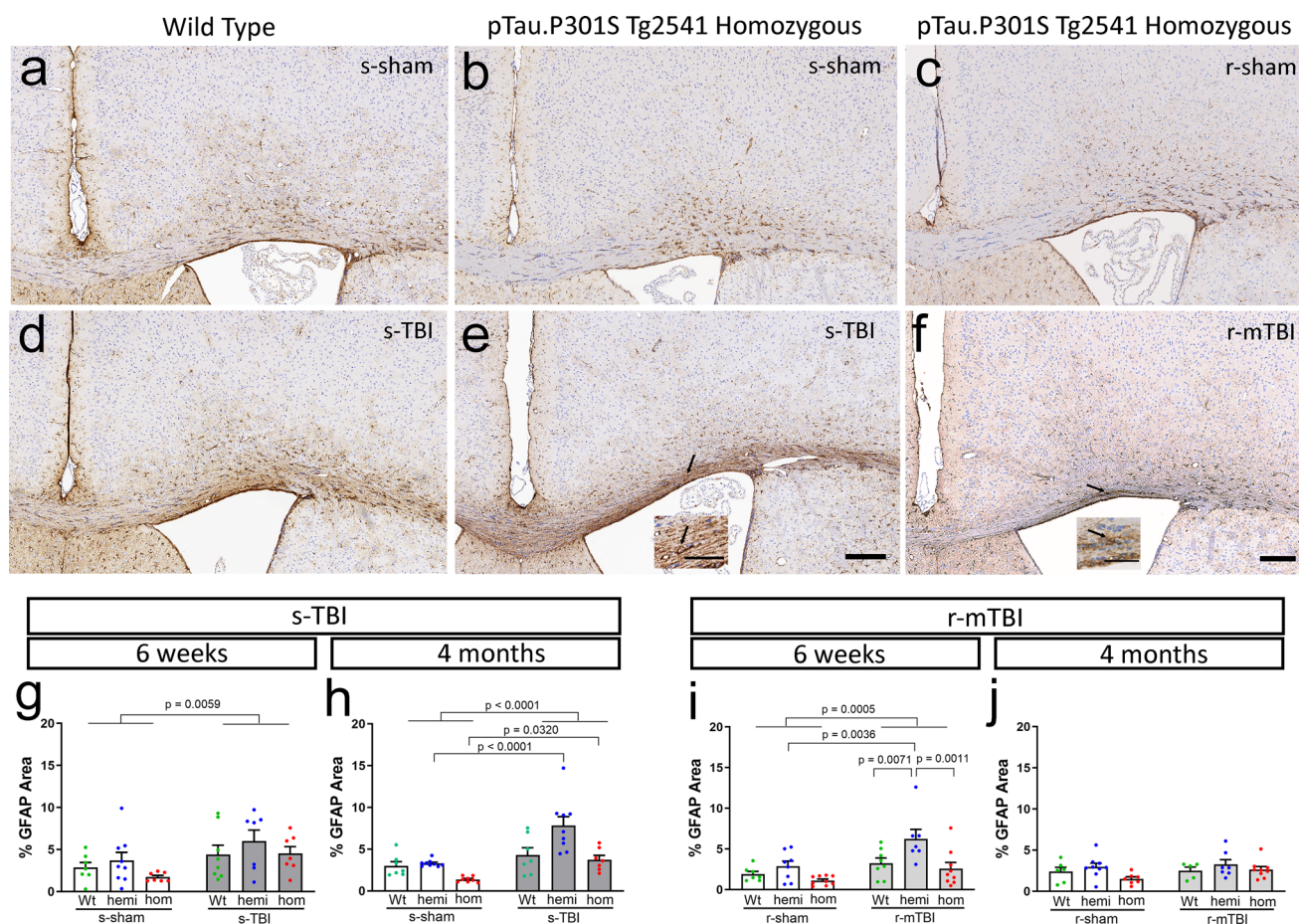


Fig. 12 Both s-TBI and r-mTBI injuries induced reactive astrogliosis in the corpus callosum, which resolved in the chronic phase after r-mTBI. **a–f** Immunohistochemistry for GFAP to identify astrocytes in coronal sections under the impact site. Nuclei stained blue with hematoxylin. Images shown are 4 months post-injury or sham procedures. Scale bars inset 50 μ m, panel images 200 μ m. **a–c** Astrocyte immunolabeling appeared similar in the cortex and corpus callosum of sham wild-type (**a**) and tau homozygous mice (**b**, **c**). **d–f** Astrogliosis in the corpus callosum was evident at 4 months after s-TBI (**c**, **e**) but localized to a more limited region after r-mTBI (**f**). **g–j** Quantification of GFAP immunolabeling in the corpus callosum shows a

main effect of injury at 6 weeks after s-TBI (**g**) and r-mTBI (**i**) that persists to 4 months after s-TBI (**h**) but resolves after r-mTBI (**j**). The tau homozygous genotype does not significantly increase astrogliosis in either injury models or at either post-injury time point. Corresponding quantification of GFAP immunolabeling in the cortex under the impact site is shown in Supplemental Information Fig. SI-5. Dots represent individual mice with wild type (Wt) in green, hemizygous (hemi) in blue, and homozygous (hom) in red. Non-significant comparisons are not shown. See Supplemental Information for full statistical analysis provided in Tables SI-6, SI-7, along with analysis that shows a lack of sex differences

of myelinated axons and/or loss of the myelin sheath along surviving axons. Our previous studies using electron microscopy for more specific and sensitive analysis of axon and myelin pathology identified a dispersed pattern of demyelination of intact axons within the corpus callosum after s-TBI [54, 56, 77]. Additional axon pathology is associated with disorganization of the molecular components of the node of Ranvier and the flanking paranodes, where myelin sheaths attach to axons. Node of Ranvier abnormalities have been identified in this s-TBI mouse model, in a swine rotational TBI model, and in human TBI cases [54, 63, 73]. Demyelination can lead to further neurodegeneration since myelination protects vulnerable denuded axons and provides bioenergetic and trophic support [50, 66], which is of interest in

neurodegenerative processes of Alzheimer's disease [52]. Furthermore, myelin is highly enriched in cholesterol, which is emerging with apolipoprotein E as an important factor in white matter impairment in aging and neurodegenerative diseases [6, 8, 69]. Axon damage (Fig. 2) and reduced myelination (Fig. 10) were also present in the cortex of tau homozygous mice after both s-sham and s-TBI procedures. In a pilot postmortem study of patients with Alzheimer's disease, cortical neuron tau pathology was associated with myelin rarefaction and small vessel disease in frontal, but not posterior, white matter and may contribute to MRI white matter hyperintensities [55]. These clinical findings provide potential relevance for neuronal tau pathology in homozygous Tg2541 mice to contribute to late-phase progression of

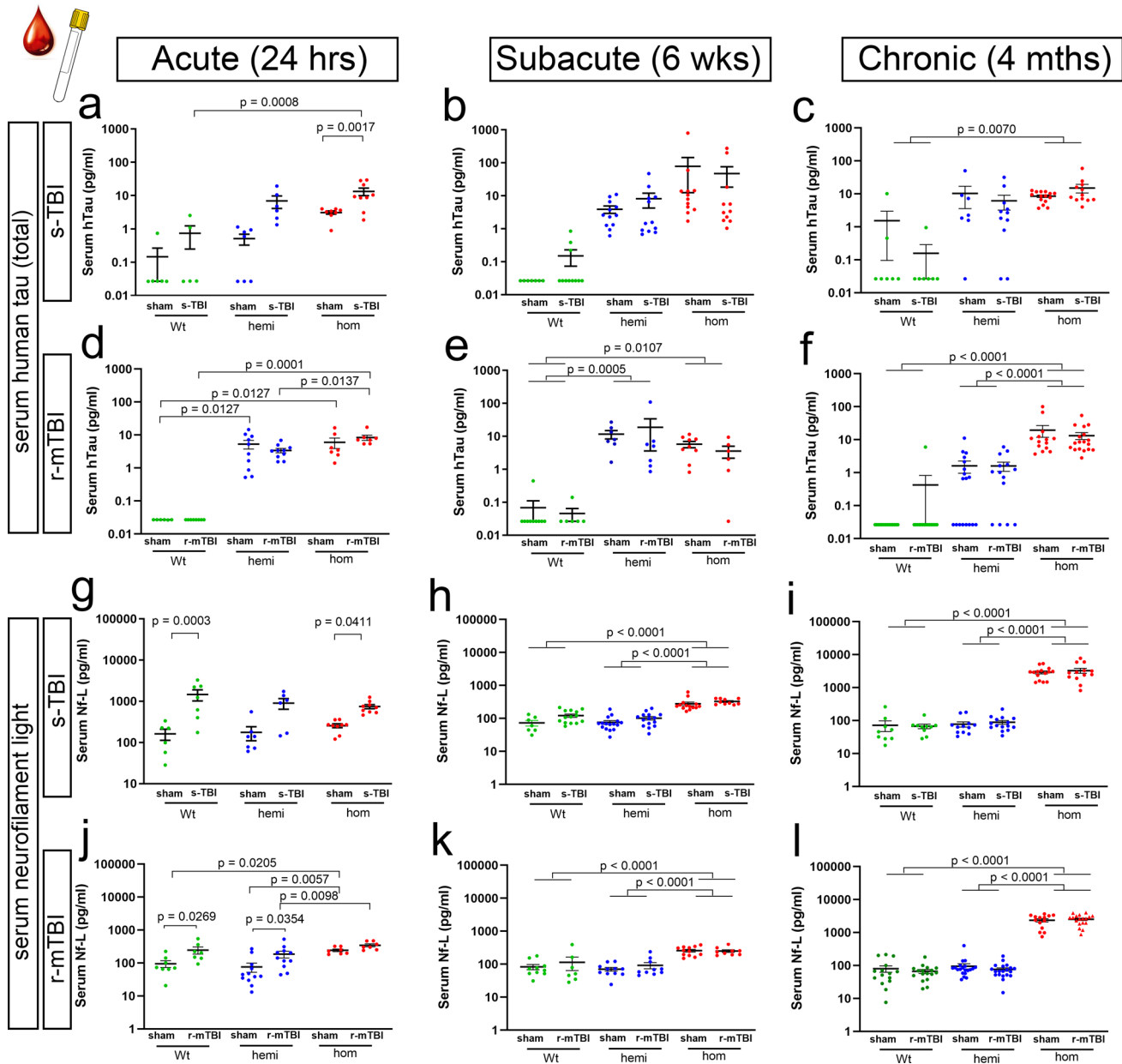


Fig. 13 Clinically used blood biomarker assay shows persistent elevation of human mutant tau while mouse neurofilament light detects axonal injury. **a–l** Mouse serum analysis using Simoa® Neurology 4-Plex A to simultaneously detect human total tau and mouse neurofilament light (Nf-L) protein levels. Dots represent individual mice with wild type (Wt) in green, hemizygous (hemi) in blue, and homozygous (hom) in red. Non-significant comparisons are not shown. Full details of statistical analysis in Table SI-6. **a** In the acute phase, tau protein levels were elevated after s-TBI in serum from homozygous Tg2541 mice, as compared to matched sham mice or to s-TBI wild-type mice. **b, c** At subacute and chronic time points, human tau protein levels were consistently elevated in s-sham and

s-TBI homozygous mice. **d–f** Human tau protein levels were consistently elevated in r-sham and r-mTBI mice. In contrast to s-TBI mice, the r-mTBI mice did not show an effect of injury in the acute phase. **g, j** In the acute phase, mouse Nf-L protein levels in serum showed a significant injury effect, which was most pronounced after s-TBI in wild-type mice. **h–i, k–l** Nf-L showed a significant increase in sham and injured homozygous mice that was similar in s-TBI and r-mTBI cohorts. The subacute elevation of Nf-L in homozygous mice further increased at the chronic stage. See Supplemental Information for full statistical analysis provided in Table SI-9, which includes analysis showing a general lack of sex differences

rostral white matter pathology after s-TBI. Further studies are warranted to include cerebrovascular pathology, which may also impact the neurovascular unit, the blood–brain barrier, and tau clearance.

Neuroinflammation is a critical factor in white matter degeneration after TBI and in other neurodegenerative diseases [19, 21, 36, 60]. Microglial activation can persist for years after a TBI with continued axon degeneration, which is associated with corpus callosum atrophy [44]. In agreement with these reports, the microglial response in the corpus callosum was exacerbated in tau homozygous mice after s-TBI and r-mTBI (Fig. 11), indicating a potential role in the interaction of tau and TBI in white matter atrophy, demyelination, and/or neuroinflammation.

Interpretation of microglial activation in the current results in Tg2541 mice, with hTau.P301S expressed in neurons from the Thy1.2 promoter, may gain from comparison with the PS19 mice, which have hTau.P301S expressed in multiple cell types from the murine prion promoter (Table SI-1). In the absence of injury, adult PS19 mice appear to have broad robust microglial activation in the brain [89]. In contrast, in our studies of sham mice, the microglial response was not different across wild-type, hemizygous or homozygous Tg2541 genotypes (Fig. 11). However, in agreement with our post-injury results, repetitive closed head injury increased the microglial response in PS19 mice [42]. The PS19 prion promoter may be advantageous in the context of tau spreading, which was accelerated after a moderate-severe penetrating TBI, and resulted in learning and memory impairment [22]. We conducted initial neurobehavioral testing based on social interaction with the 3-chamber assessment that differentiated r-mTBI effects in wild-type mice in our prior study [90]. However, the tau genotype in hemizygous Tg2541 mice impaired social interaction in sham mice to a similar extent as r-mTBI in wild-type mice (Figure SI-4), indicating that even this lower level of hemizygous mutant tau can obscure neurobehavioral assessments of an injury effect. The current results from analysis of atrophy, neuroinflammation, and demyelination in the corpus callosum white matter are further supported by the effects of P301S hTau expression in a repetitive model (Table SI-1) that involved mainly the optic nerve and tract [16].

The experiments in this study included male and female mice with analysis of sex as a biological variable provided within the Supplemental Information (Tables SI-1 through SI-9). A prior study focused on the kinetics of tau prion formation from hTau.P301S Tg2541 mice observed that after a similar onset of neurologic deficits in males and females at approximately 24 weeks of age, degeneration progressed slightly more rapidly in females [85]. This prior data and the hang time deficits observed herein support selection of the chronic time point at 4 months post-injury, which is approximately 24 weeks of age with the mice injured at 8 weeks of

age (Fig. 1). We found that males generally weighed more than females (Table SI-1), which may have contributed to a sex difference among hemizygous mice in the neurologic assessment after injury using the hang time test (Table SI-4). The main findings of the study develop by the 4-month time point in homozygous mice, for which sex differences were not detected. The most prominent sex difference was higher IBA1 in the corpus callosum of female homozygous mice at 6 weeks after s-TBI (Table SI-6).

There are several limitations that should be considered in the interpretation of these results. The Neurology 4-Plex A was an informative and translational approach with the advantage of simultaneous analysis of human tau and mouse neurofilament light proteins in a given sample (Fig. 13). In addition, while an injury effect was discerned at the acute time point, serum levels are not specific to effects in the brain since neuronal expression of human mutant tau is expressed broadly, including in the spinal cord (Fig. SI-6). The performance data of the Neurology 4-Plex A for mouse GFAP and UCHL-1 were not available during our initial studies. Future testing may be more sensitive for neurofilament light with a single assay format, while GFAP and UCHL-1 assays would need to be designed specifically for mouse proteins. Another limitation is that mouse models cannot provide a full range of injury parameters that may be important in human TBI. The two closed head TBI mouse models in this study reflect key pathological features of single moderate TBI and repetitive mild TBI as two main forms of human TBI; each model was previously characterized by neuropathology, fluorescent reporter mice, MRI structural and diffusion tensor imaging, and behavioral assessments. In our analysis, the range of neuropathology created using the two models was advantageous for identifying multiple chronic phase effects of tau. Future studies in other models could capture additional pathological features, such as traumatic vascular injury and gyrencephalic structure.

Conclusion

To our knowledge, this study is the first demonstration that modifying neuronal tau worsens late-stage TBI neuropathological sequelae in the corpus callosum, a major white matter tract associated with clinical evaluation of post-traumatic neurodegeneration. Our results show a significant impact of phosphorylated tau pathology on corpus callosum atrophy, demyelination, and neuroinflammation in the progression from the subacute to chronic phase TBI. The results reveal an interplay of the tau modification and the extent of TBI pathology over the post-injury time course. These findings support the applicability of mouse models for identifying potential therapeutics to mitigate neuropathological sequelae of TBI. Further studies would be needed to determine the

extent to which the tau mutation in Tg2541 mice represents a more generalizable, while potentially accelerated, interplay of pathological tau in neuropathological sequelae after TBI. Large-scale phosphoproteomic network analysis in this Tg2541 mouse strain revealed protein co-expression modules associated with tau-induced pathologies, with specific tau phosphorylation sites related to the neuroinflammatory response, mitochondrial bioenergetic processes, cholesterol biosynthesis, and postsynaptic density [81]. These modules and networks are also relevant to TBI pathologies. Therefore, future studies leveraging the current results could provide further insight into factors leading to post-traumatic neurodegeneration and potential targets for screening novel therapeutics.

Supplementary Information The online version contains supplementary material available at <https://doi.org/10.1007/s00401-023-02622-9>.

Acknowledgements We are grateful to Dr. Tony Wyss-Coray (Stanford University, California, USA) for providing mice to initiate our hTau. P301S Tg2541 colony. We appreciate assistance from core resources including the Preclinical Behavior and Models Core, Biomarkers Core, and Translational Therapeutics Core of the Center for Neuroscience and Regenerative Medicine (renamed as Military Traumatic Brain Injury Initiative) and The American Genome Center. We thank Drs. Kryslaine Radomski and Genevieve Sullivan for helpful comments on the manuscript.

Author contributions The study concept was developed and designed by RA and DP. Experiments were designed by FY and RA. Material preparation, data collection and analysis were performed by FY, DI, CL, JG, TL, PL, GS, and RA. The first draft of the manuscript was written by FY and RA and all the authors commented on previous versions of the manuscript. All the authors read and approved the final manuscript.

Funding The study was supported by United States Defense Health Agency Program in Brain Injury and Disease Prevention, Treatment, and Research (HU0001-22-2-0002).

Data availability This study did not generate big data resources but data from specific experiments will be made available upon request and statistical data from the current experiments is provided as Supplementary Information.

Declarations

Conflict of interest The authors have no conflicts of interest to disclose. The views, information or content, and conclusions presented do not necessarily represent the official position or policy of, nor should any official endorsement be inferred on the part of, the Uniformed Services University, the Department of Defense, the U.S. Government or the Henry M. Jackson Foundation for the Advancement of Military Medicine, Inc.

Open Access This article is licensed under a Creative Commons Attribution 4.0 International License, which permits use, sharing, adaptation, distribution and reproduction in any medium or format, as long as you give appropriate credit to the original author(s) and the source, provide a link to the Creative Commons licence, and indicate if changes were made. The images or other third party material in this article are included in the article's Creative Commons licence, unless indicated

otherwise in a credit line to the material. If material is not included in the article's Creative Commons licence and your intended use is not permitted by statutory regulation or exceeds the permitted use, you will need to obtain permission directly from the copyright holder. To view a copy of this licence, visit <http://creativecommons.org/licenses/by/4.0/>.

References

- Adamek GD, Shipley MT, Sanders MS (1984) The indusium griseum in the mouse: architecture, Timm's histochemistry and some afferent connections. *Brain Res Bull* 12:657–668. [https://doi.org/10.1016/0361-9230\(84\)90147-3](https://doi.org/10.1016/0361-9230(84)90147-3)
- Allen B, Ingram E, Takao M, Smith MJ, Jakes R, Virdee K et al (2002) Abundant tau filaments and nonapoptotic neurodegeneration in transgenic mice expressing human P301S tau protein. *J Neurosci* 22:9340–9351
- Alosco ML, Stein TD, Tripodis Y, Chua AS, Kowall NW, Huber BR et al (2019) Association of white matter rarefaction, arteriolosclerosis, and tau with dementia in chronic traumatic encephalopathy. *JAMA Neurol* 76:1298–1308. <https://doi.org/10.1001/jamanneurol.2019.2244>
- Andorfer C, Kress Y, Espinoza M, de Silva R, Tucker KL, Barde YA et al (2003) Hyperphosphorylation and aggregation of tau in mice expressing normal human tau isoforms. *J Neurochem* 86:582–590. <https://doi.org/10.1046/j.1471-4159.2003.01879.x>
- Bachstetter AD, Morganti JM, Bodnar CN, Webster SJ, Higgins EK, Roberts KN et al (2020) The effects of mild closed head injuries on tauopathy and cognitive deficits in rodents: primary results in wild type and rTg4510 mice, and a systematic review. *Exp Neurol* 326:113180. <https://doi.org/10.1016/j.expneurol.2020.113180>
- Berghoff SA, Spieth L, Saher G (2022) Local cholesterol metabolism orchestrates remyelination. *Trends Neurosci* 45:272–283. <https://doi.org/10.1016/j.tins.2022.01.001>
- Bernick C, Shan G, Zetterberg H, Banks S, Mishra VR, Bekris L et al (2020) Longitudinal change in regional brain volumes with exposure to repetitive head impacts. *Neurology* 94:e232–e240. <https://doi.org/10.1212/WNL.0000000000008817>
- Blanchard JW, Akay LA, Davila-Velderrain J, von Maydell D, Mathys H, Davidson SM et al (2022) APOE4 impairs myelination via cholesterol dysregulation in oligodendrocytes. *Nature* 611:769–779. <https://doi.org/10.1038/s41586-022-05439-w>
- Bohyn C, Vyvere TV, Keyzer F, Sima DM, Demaerel P (2022) Morphometric evaluation of traumatic axonal injury and the correlation with post-traumatic cerebral atrophy and functional outcome. *Neuroradiol J* 35:468–476. <https://doi.org/10.1177/197140092111049714>
- Bradshaw DV Jr, Knutsen AK, Korotcov A, Sullivan GM, Radomski KL, Dardzinski BJ et al (2021) Genetic inactivation of SARM1 axon degeneration pathway improves outcome trajectory after experimental traumatic brain injury based on pathological, radiological, and functional measures. *Acta Neuropathol Commun* 9:89. <https://doi.org/10.1186/s40478-021-01193-8>
- Braun NJ, Yao KR, Alford PW, Liao D (2020) Mechanical injuries of neurons induce tau mislocalization to dendritic spines and tau-dependent synaptic dysfunction. *Proc Natl Acad Sci U S A* 117:29069–29079. <https://doi.org/10.1073/pnas.2008306117>
- Brett BL, Gardner RC, Godbout J, Dams-O'Connor K, Keene CD (2022) Traumatic brain injury and risk of neurodegenerative disorder. *Biol Psychiatry* 91:498–507. <https://doi.org/10.1016/j.biopsych.2021.05.025>
- Brodal A (1947) The hippocampus and the sense of smell; a review. *Brain* 70:179–222. <https://doi.org/10.1093/brain/70.2.179>

14. Castano-Leon AM, Sanchez Carabias C, Hilario A, Ramos A, Navarro-Main B, Paredes I et al (2023) Serum assessment of traumatic axonal injury: the correlation of GFAP, t-Tau, UCH-L1, and NfL levels with diffusion tensor imaging metrics and its prognosis utility. *J Neurosurg* 138:454–464. <https://doi.org/10.3171/2022.5.JNS22638>
15. Chancellor KB, Chancellor SE, Duke-Cohan JE, Huber BR, Stein TD, Alvarez VE et al (2021) Altered oligodendroglia and astroglia in chronic traumatic encephalopathy. *Acta Neuropathol* 142:295–321. <https://doi.org/10.1007/s00401-021-02322-2>
16. Cheng H, Deaton LM, Qiu M, Ha S, Pacoma R, Lao J et al (2020) Tau overexpression exacerbates neuropathology after repeated mild head impacts in male mice. *Neurobiol Dis* 134:104683. <https://doi.org/10.1016/j.nbd.2019.104683>
17. Chon U, Vanselow DJ, Cheng KC, Kim Y (2019) Enhanced and unified anatomical labeling for a common mouse brain atlas. *Nat Commun* 10:5067. <https://doi.org/10.1038/s41467-019-13057-w>
18. Cowan CM, Mudher A (2013) Are tau aggregates toxic or protective in tauopathies? *Front Neurol* 4:114. <https://doi.org/10.3389/fneur.2013.00114>
19. Daneshvar DH, Goldstein LE, Kiernan PT, Stein TD, McKee AC (2015) Post-traumatic neurodegeneration and chronic traumatic encephalopathy. *Mol Cell Neurosci*. <https://doi.org/10.1016/j.mcn.2015.03.007>
20. Delobel P, Lavenir I, Fraser G, Ingram E, Holzer M, Ghetti B et al (2008) Analysis of tau phosphorylation and truncation in a mouse model of human tauopathy. *Am J Pathol* 172:123–131. <https://doi.org/10.2353/ajpath.2008.070627>
21. Devanney NA, Stewart AN, Gensel JC (2020) Microglia and macrophage metabolism in CNS injury and disease: the role of immunometabolism in neurodegeneration and neurotrauma. *Exp Neurol* 329:113310. <https://doi.org/10.1016/j.expneurol.2020.113310>
22. Edwards G 3rd, Zhao J, Dash PK, Soto C, Moreno-Gonzalez I (2020) Traumatic brain injury induces tau aggregation and spreading. *J Neurotrauma* 37:80–92. <https://doi.org/10.1089/neu.2018.6348>
23. Feng G, Mellor RH, Bernstein M, Keller-Peck C, Nguyen QT, Wallace M et al (2000) Imaging neuronal subsets in transgenic mice expressing multiple spectral variants of GFP. *Neuron* 28:41–51. [https://doi.org/10.1016/s0896-6273\(00\)00084-2](https://doi.org/10.1016/s0896-6273(00)00084-2)
24. Figley MD, DiAntonio A (2020) The SARM1 axon degeneration pathway: control of the NAD(+) metabolome regulates axon survival in health and disease. *Curr Opin Neurobiol* 63:59–66. <https://doi.org/10.1016/j.conb.2020.02.012>
25. Foster NN, Barry J, Korobkova L, Garcia L, Gao L, Becerra M et al (2021) The mouse cortico-basal ganglia-thalamic network. *Nature* 598:188–194. <https://doi.org/10.1038/s41586-021-03993-3>
26. Frost EE, Nielsen JA, Le TQ, Armstrong RC (2003) PDGF and FGF2 regulate oligodendrocyte progenitor responses to demyelination. *J Neurobiol* 54:457–472. <https://doi.org/10.1002/neu.10158>
27. Gangolli M, Benetatos J, Esparza TJ, Fountain EM, Seneviratne S, Brody DL (2019) Repetitive concussive and subconcussive injury in a human tau mouse model results in chronic cognitive dysfunction and disruption of white matter tracts, but not tau pathology. *J Neurotrauma* 36:735–755. <https://doi.org/10.1089/neu.2018.5700>
28. Gehrman J, Banati RB, Cuzner ML, Kreutzberg GW, Newcombe J (1995) Amyloid precursor protein (APP) expression in multiple sclerosis lesions. *Glia* 15:141–151. <https://doi.org/10.1002/glia.440150206>
29. Gill J, Latour L, Diaz-Arrastia R, Motamedi V, Turtzo C, Shahim P et al (2018) Glial fibrillary acidic protein elevations relate to neuroimaging abnormalities after mild TBI. *Neurology* 91:e1385–e1389. <https://doi.org/10.1212/WNL.0000000000006321>
30. Goldstein LE, Fisher AM, Tagge CA, Zhang XL, Velisek L, Sullivan JA et al (2012) Chronic traumatic encephalopathy in blast-exposed military veterans and a blast neurotrauma mouse model. *Sci Transl Med* 4:134ra160. <https://doi.org/10.1126/scitranslmed.3003716>
31. Gotz J, Halliday G, Nisbet RM (2019) Molecular pathogenesis of the tauopathies. *Annu Rev Pathol* 14:239–261. <https://doi.org/10.1146/annurev-pathmechdis-012418-012936>
32. Graham NSN, Cole JH, Bourke NJ, Schott JM, Sharp DJ (2023) Distinct patterns of neurodegeneration after TBI and in Alzheimer's disease. *Alzheimers Dement*. <https://doi.org/10.1002/alz.12934>
33. Graham NSN, Jolly A, Zimmerman K, Bourke NJ, Scott G, Cole JH et al (2020) Diffuse axonal injury predicts neurodegeneration after moderate-severe traumatic brain injury. *Brain* 143:3685–3698. <https://doi.org/10.1093/brain/awaa316>
34. Graham NSN, Zimmerman KA, Moro F, Heslegrave A, Maillard SA, Bernini A et al (2021) Axonal marker neurofilament light predicts long-term outcomes and progressive neurodegeneration after traumatic brain injury. *Sci Transl Med* 13:eabg9922. <https://doi.org/10.1126/scitranslmed.abg9922>
35. Gray E, Rice C, Nightingale H, Ginty M, Hares K, Kemp K et al (2013) Accumulation of cortical hyperphosphorylated neurofilaments as a marker of neurodegeneration in multiple sclerosis. *Mult Scler* 19:153–161. <https://doi.org/10.1177/1352458512451661>
36. Grovola MR, von Reyn C, Loane DJ, Cullen DK (2023) Understanding microglial responses in large animal models of traumatic brain injury: an underutilized resource for preclinical and translational research. *J Neuroinflammation* 20:67. <https://doi.org/10.1186/s12974-023-02730-z>
37. Havlicek DF, Fuhang R, Nikulina E, Smith-Salzberg B, Lawless S, Severin SA et al (2023) A single closed head injury in male adult mice induces chronic, progressive white matter atrophy and increased phospho-tau expressing oligodendrocytes. *Exp Neurol* 359:114241. <https://doi.org/10.1016/j.expneurol.2022.114241>
38. Holper S, Watson R, Yassi N (2022) Tau as a biomarker of neurodegeneration. *Int J Mol Sci*. <https://doi.org/10.3390/ijms23137307>
39. Hoover BR, Reed MN, Su J, Penrod RD, Kotilinek LA, Grant MK et al (2010) Tau mislocalization to dendritic spines mediates synaptic dysfunction independently of neurodegeneration. *Neuron* 68:1067–1081. <https://doi.org/10.1016/j.neuron.2010.11.030>
40. Hsu JL, Wei YC, Toh CH, Hsiao IT, Lin KJ, Yen TC et al (2023) Magnetic resonance images implicate that glymphatic alterations mediate cognitive dysfunction in Alzheimer disease. *Ann Neurol* 93:164–174. <https://doi.org/10.1002/ana.26516>
41. Ishida K, Yamada K, Nishiyama R, Hashimoto T, Nishida I, Abe Y et al (2022) Glymphatic system clears extracellular tau and protects from tau aggregation and neurodegeneration. *J Exp Med*. <https://doi.org/10.1084/jem.20211275>
42. Izzy S, Brown-Whalen A, Yahya T, Sarro-Schwartz A, Jin G, Chung JY et al (2021) Repetitive traumatic brain injury causes neuroinflammation before tau pathology in adolescent P301S mice. *Int J Mol Sci*. <https://doi.org/10.3390/ijms22020907>
43. Johnson NR, Condello C, Guan S, Oehler A, Becker J, Gavidia M et al (2017) Evidence for sortilin modulating regional accumulation of human tau prions in transgenic mice. *Proc Natl Acad Sci U S A* 114:E11029–E11036. <https://doi.org/10.1073/pnas.1717193114>
44. Johnson VE, Stewart JE, Begbie FD, Trojanowski JQ, Smith DH, Stewart W (2013) Inflammation and white matter degeneration persist for years after a single traumatic brain injury. *Brain* 136:28–42. <https://doi.org/10.1093/brain/aws322>
45. Kahrman A, Bouley J, Smith TW, Bosco DA, Woerman AL, Henninger N (2021) Mouse closed head traumatic brain injury

- replicates the histological tau pathology pattern of human disease: characterization of a novel model and systematic review of the literature. *Acta Neuropathol Commun* 9:118. <https://doi.org/10.1186/s40478-021-01220-8>
46. Kennedy E, Panahi S, Stewart IJ, Tate DF, Wilde EA, Kenney K et al (2022) Traumatic brain injury and early onset dementia in post 9–11 veterans. *Brain Inj* 36:620–627. <https://doi.org/10.1080/02699052.2022.2033846>
 47. Korley FK, Yue JK, Wilson DH, Hrusovsky K, Diaz-Arrastia R, Ferguson AR et al (2018) Performance evaluation of a multiplex assay for simultaneous detection of four clinically relevant traumatic brain injury biomarkers. *J Neurotrauma* 36:182–187. <https://doi.org/10.1089/neu.2017.5623>
 48. Kubo A, Misonou H, Matsuyama M, Nomori A, Wada-Kakuda S, Takashima A et al (2019) Distribution of endogenous normal tau in the mouse brain. *J Comp Neurol* 527:985–998. <https://doi.org/10.1002/cne.24577>
 49. Lange RT, Lippa S, Brickell TA, Gill J, French LM (2023) Serum tau, neurofilament light chain, glial fibrillary acidic protein, and ubiquitin carboxyl-terminal hydrolase L1 are associated with the chronic deterioration of neurobehavioral symptoms after traumatic brain injury. *J Neurotrauma* 40:482–492. <https://doi.org/10.1089/neu.2022.0249>
 50. Li S, Sheng ZH (2023) Oligodendrocyte-derived transcellular signaling regulates axonal energy metabolism. *Curr Opin Neurobiol* 80:102722. <https://doi.org/10.1016/j.conb.2023.102722>
 51. Lyall DM, Russell ER, Ward J, Stewart W (2022) History of traumatic brain injury is associated with impaired cognition and imaging evidence of altered white matter tract integrity in UK Biobank UK Biobank. <https://doi.org/10.31234/osf.io/7wb9n>
 52. Maitre M, Jeltsch-David H, Okechukwu NG, Klein C, Patte-Mensah C, Mensah-Nyagan AG (2023) Myelin in Alzheimer's disease: culprit or bystander? *Acta Neuropathol Commun* 11:56. <https://doi.org/10.1186/s40478-023-01554-5>
 53. Marion CM, McDaniel DP, Armstrong RC (2019) Sarm1 deletion reduces axon damage, demyelination, and white matter atrophy after experimental traumatic brain injury. *Exp Neurol* 321:113040. <https://doi.org/10.1016/j.expneurol.2019.113040>
 54. Marion CM, Radomski KL, Cramer NP, Galdzicki Z, Armstrong RC (2018) Experimental traumatic brain injury identifies distinct early and late phase axonal conduction deficits of white matter pathophysiology, and reveals intervening recovery. *J Neurosci* 38:8723–8736. <https://doi.org/10.1523/JNEUROSCI.0819-18.2018>
 55. McAleese KE, Miah M, Graham S, Hadfield GM, Walker L, Johnson M et al (2021) Frontal white matter lesions in Alzheimer's disease are associated with both small vessel disease and AD-associated cortical pathology. *Acta Neuropathol* 142:937–950. <https://doi.org/10.1007/s00401-021-02376-2>
 56. Mierzwa AJ, Marion CM, Sullivan GM, McDaniel DP, Armstrong RC (2015) Components of myelin damage and repair in the progression of white matter pathology after mild traumatic brain injury. *J Neuropathol Exp Neurol* 74:218–232. <https://doi.org/10.1097/NEN.0000000000000165>
 57. Moro F, Lisi I, Tolomeo D, Vegliante G, Pascente R, Mazzone E et al (2023) Acute blood levels of neurofilament light indicate one-year white matter pathology and functional impairment in repetitive mild traumatic brain injured mice. *J Neurotrauma*. <https://doi.org/10.1089/neu.2022.0252>
 58. Mouzon B, Bachmeier C, Ojo J, Acker C, Ferguson S, Crynen G et al (2019) Chronic white matter degeneration, but no tau pathology at one-year post-repetitive mild traumatic brain injury in a tau transgenic model. *J Neurotrauma* 36:576–588. <https://doi.org/10.1089/neu.2018.5720>
 59. Mouzon BC, Bachmeier C, Ferro A, Ojo JO, Crynen G, Acker CM et al (2014) Chronic neuropathological and neurobehavioral changes in a repetitive mild traumatic brain injury model. *Ann Neurol* 75:241–254. <https://doi.org/10.1002/ana.24064>
 60. Needham EJ, Helmy A, Zanier ER, Jones JL, Coles AJ, Menon DK (2019) The immunological response to traumatic brain injury. *J Neuroimmunol* 332:112–125. <https://doi.org/10.1016/j.jneuroim.2019.04.005>
 61. Newcombe VFJ, Ashton NJ, Posti JP, Glocker B, Manktelow A, Chatfield DA et al (2022) Post-acute blood biomarkers and disease progression in traumatic brain injury. *Brain* 145:2064–2076. <https://doi.org/10.1093/brain/awac126>
 62. Portillo E, Zi X, Kim Y, Tucker LB, Fu A, Miller LA et al (2023) Persistent hypersomnia following repetitive mild experimental traumatic brain injury: Roles of chronic stress and sex differences. *J Neurosci Res* 101:843–865. <https://doi.org/10.1002/jnr.25165>
 63. Radomski KL, Zi X, Lischka FW, Noble MD, Galdzicki Z, Armstrong RC (2022) Acute axon damage and demyelination are mitigated by 4-aminopyridine (4-AP) therapy after experimental traumatic brain injury. *Acta Neuropathol Commun* 10:67. <https://doi.org/10.1186/s40478-022-01366-z>
 64. Reber J, Hwang K, Bowren M, Bruss J, Mukherjee P, Tranel D et al (2021) Cognitive impairment after focal brain lesions is better predicted by damage to structural than functional network hubs. *Proc Natl Acad Sci U S A*. <https://doi.org/10.1073/pnas.2018784118>
 65. Redwine JM, Armstrong RC (1998) In vivo proliferation of oligodendrocyte progenitors expressing PDGFalphaR during early remyelination. *J Neurobiol* 37:413–428. [https://doi.org/10.1002/\(SICI\)1097-4695\(19981115\)37:3%3c413::AID-NEU7%3e3.0.CO;2-8\[pil\]](https://doi.org/10.1002/(SICI)1097-4695(19981115)37:3%3c413::AID-NEU7%3e3.0.CO;2-8[pil])
 66. Saab AS, Nave KA (2017) Myelin dynamics: protecting and shaping neuronal functions. *Curr Opin Neurobiol* 47:104–112. <https://doi.org/10.1016/j.conb.2017.09.013>
 67. Sambashivan S, Freeman MR (2021) SARM1 signaling mechanisms in the injured nervous system. *Curr Opin Neurobiol* 69:247–255. <https://doi.org/10.1016/j.conb.2021.05.004>
 68. Shahim P, Politis A, van der Merwe A, Moore B, Ekanayake V, Lippa SM et al (2020) Time course and diagnostic utility of NfL, tau, GFAP, and UCH-L1 in subacute and chronic TBI. *Neurology* 95:e623–e636. <https://doi.org/10.1212/WNL.00000000000009985>
 69. Sharp FR, DeCarli CS, Jin LW, Zhan X (2023) White matter injury, cholesterol dysmetabolism, and APP/Abeta dysmetabolism interact to produce Alzheimer's disease (AD) neuropathology: a hypothesis and review. *Front Aging Neurosci* 15:1096206. <https://doi.org/10.3389/fnagi.2023.1096206>
 70. Sherman MA, LaCroix M, Amar F, Larson ME, Forster C, Aguzzi A et al (2016) Soluble conformers of abeta and tau alter selective proteins governing axonal transport. *J Neurosci* 36:9647–9658. <https://doi.org/10.1523/JNEUROSCI.1899-16.2016>
 71. Shively SB, Edgerton SL, Iacono D, Purohit DP, Qu BX, Haroutunian V et al (2017) Localized cortical chronic traumatic encephalopathy pathology after single, severe axonal injury in human brain. *Acta Neuropathol* 133:353–366. <https://doi.org/10.1007/s00401-016-1649-7>
 72. Song H, Chen C, Kelley B, Tomasevich A, Lee H, Dolle JP et al (2022) Traumatic brain injury recapitulates developmental changes of axons. *Prog Neurobiol* 217:102332. <https://doi.org/10.1016/j.pneurobio.2022.102332>
 73. Song H, McEwan PP, Ameen-Ali KE, Tomasevich A, Kennedy-Dietrich C, Palma A et al (2022) Concussion leads to widespread axonal sodium channel loss and disruption of the node of Ranvier. *Acta Neuropathol* 144:967–985. <https://doi.org/10.1007/s00401-022-02498-1>
 74. Soppela H, Kruger J, Hartikainen P, Koivisto A, Haapasalo A, Borroni B et al (2023) Traumatic brain injury associates with an

- earlier onset in sporadic frontotemporal dementia. *J Alzheimers Dis* 91:225–232. <https://doi.org/10.3233/JAD-220545>
75. Sternberger LA, Sternberger NH (1983) Monoclonal antibodies distinguish phosphorylated and nonphosphorylated forms of neurofilaments in situ. *Proc Natl Acad Sci U S A* 80:6126–6130. <https://doi.org/10.1073/pnas.80.19.6126>
 76. Strich SJ (1956) Diffuse degeneration of the cerebral white matter in severe dementia following head injury. *J Neurol Neurosurg Psychiatry* 19:163–185
 77. Sullivan GM, Mierzwa AJ, Kijpaisalratana N, Tang H, Wang Y, Song SK et al (2013) Oligodendrocyte lineage and subventricular zone response to traumatic axonal injury in the corpus callosum. *J Neuropathol Exp Neurol* 72:1106–1125. <https://doi.org/10.1097/NEN.0000000000000009>
 78. Tobin JE, Xie M, Le TQ, Song SK, Armstrong RC (2011) Reduced axonopathy and enhanced remyelination after chronic demyelination in fibroblast growth factor 2 (Fgf2)-null mice: differential detection with diffusion tensor imaging. *J Neuropathol Exp Neurol* 70:157–165. <https://doi.org/10.1097/NEN.0b013e31820937e4>
 79. Torii T, Miyamoto Y, Nakata R, Higashi Y, Shinmyo Y, Kawasaki H et al (2023) Identification of Tau protein as a novel marker for maturation and pathological changes of oligodendrocytes. *Glia* 71:1002–1017. <https://doi.org/10.1002/glia.24322>
 80. Trapp BD, Peterson J, Ransohoff RM, Rudick R, Mork S, Bo L (1998) Axonal transection in the lesions of multiple sclerosis. *N Engl J Med* 338:278–285
 81. Tsumagari K, Sato Y, Shimozawa A, Aoyagi H, Okano H, Kuromitsu J (2022) Co-expression network analysis of human tau-transgenic mice reveals protein modules associated with tau-induced pathologies. *iScience* 25:104832. <https://doi.org/10.1016/j.isci.2022.104832>
 82. Vacchi E, Kaelin-Lang A, Melli G (2020) Tau and Alpha Synuclein Synergistic Effect in Neurodegenerative Diseases: When the Periphery Is the Core. *Int J Mol Sci*. <https://doi.org/10.3390/ijms21145030>
 83. van Eijck M, van der Naalt J, de Jongh M, Schoonman G, Oldenbeuving A, Peluso J et al (2018) Patients with diffuse axonal injury can recover to a favorable long-term functional and quality of life outcome. *J Neurotrauma* 35:2357–2364. <https://doi.org/10.1089/neu.2018.5650>
 84. Walker A, Chapin B, Abisambra J, DeKosky ST (2022) Association between single moderate to severe traumatic brain injury and long-term tauopathy in humans and preclinical animal models: a systematic narrative review of the literature. *Acta Neuropathol Commun* 10:13. <https://doi.org/10.1186/s40478-022-01311-0>
 85. Woerman AL, Patel S, Kazmi SA, Oehler A, Freyman Y, Espiritu L et al (2017) Kinetics of human mutant tau prion formation in the brains of 2 transgenic mouse lines. *JAMA Neurol* 74:1464–1472. <https://doi.org/10.1001/jamaneurol.2017.2822>
 86. Wu M, Chen Z, Jiang M, Bao B, Li D, Yin X et al (2023) Friend or foe: role of pathological tau in neuronal death. *Mol Psychiatry*. <https://doi.org/10.1038/s41380-023-02024-z>
 87. Xu H, Rosler TW, Carlsson T, de Andrade A, Fiala O, Hollerhage M et al (2014) Tau silencing by siRNA in the P301S mouse model of tauopathy. *Curr Gene Ther* 14:343–351. <https://doi.org/10.2174/156652321405140926160602>
 88. Yasuda M, Nakamura Y, Kawamata T, Kaneyuki H, Maeda K, Komure O (2005) Phenotypic heterogeneity within a new family with the MAPT p301s mutation. *Ann Neurol* 58:920–928. <https://doi.org/10.1002/ana.20668>
 89. Yoshiyama Y, Higuchi M, Zhang B, Huang SM, Iwata N, Saido TC et al (2007) Synapse loss and microglial activation precede tangles in a P301S tauopathy mouse model. *Neuron* 53:337–351. <https://doi.org/10.1016/j.neuron.2007.01.010>
 90. Yu F, Shukla DK, Armstrong RC, Marion CM, Radomski KL, Selwyn RG et al (2017) Repetitive model of mild traumatic brain injury produces cortical abnormalities detectable by magnetic resonance diffusion imaging (DTI/DKI), histopathology, and behavior. *J Neurotrauma* 34:1364–1381. <https://doi.org/10.1089/neu.2016.4569>
 91. Yuan J, Gong H, Li A, Li X, Chen S, Zeng S et al (2015) Visible rodent brain-wide networks at single-neuron resolution. *Front Neuroanat* 9:70. <https://doi.org/10.3389/fnana.2015.00070>
 92. Zempel H, Mandelkow E (2019) Mechanisms of axonal sorting of tau and influence of the axon initial segment on tau cell polarity. *Adv Exp Med Biol* 1184:69–77. https://doi.org/10.1007/978-981-32-9358-8_6

Publisher's Note Springer Nature remains neutral with regard to jurisdictional claims in published maps and institutional affiliations.